Signatures of CD8+ T cell dysfunction in AML patients and their reversibility with response to chemotherapy

Hanna A. Knaus,[1,2] Sofia Berglund,[1] Hubert Hackl,[3] Amanda L. Blackford,[4] Joshua F. Zeidner,[1,5] Raúl Montiel-Esparza,[1] Rupkatha Mukhopadhyay,[1] Katrina Vanura,[2] Bruce R. Blazar,[6] Judith E. Karp,[1] Leo Luznik,[1] and Ivana Gojo[1]

[1]Division of Hematologic Malignances, Sidney Kimmel Comprehensive Cancer Center, Johns Hopkins University, Baltimore, Maryland, USA. [2]Division of Hematology and Hemostaseology, Department of Medicine I, Medical University of Vienna, Vienna, Austria. [3]Division of Bioinformatics, Biocenter, Medical University of Innsbruck, Innsbruck, Austria. [4]Division of Biostatistics and Bioinformatics, Sidney Kimmel Comprehensive Cancer Center, Johns Hopkins University, Baltimore, Maryland, USA. [5]Lineberger Comprehensive Cancer Center, University of North Carolina, Chapel Hill, North Carolina, USA. [6]Division of Blood and Marrow Transplantation, Department of Pediatrics, University of Minnesota, Minneapolis, Minnesota, USA.

BACKGROUND. Our understanding of phenotypic and functional signatures of CD8+ T cell dysfunction in acute myeloid leukemia (AML) is limited. Deciphering these deranged T cell functional states and how they are impacted by induction chemotherapy is essential for incorporation of novel immune-based strategies to restore and maintain antileukemia immunity.

METHODS. We utilized high-dimensional immunophenotyping, gene expression, and functional studies to characterize peripheral blood and bone marrow CD8+ T cells in 72 AML patients at diagnosis and after induction chemotherapy.

RESULTS. Our data suggest that multiple aspects of deranged T cell function are operative in AML at diagnosis, with exhaustion and senescence being the dominant processes. Following treatment, the phenotypic and transcriptional profile of CD8+ T cells diverged between responders and nonresponders. Response to therapy correlated with upregulation of costimulatory, and downregulation of apoptotic and inhibitory, T cell signaling pathways, indicative of restoration of T cell function. In functional studies, AML blasts directly altered CD8+ T cell viability, expansion, co-signaling and senescence marker expression. This CD8+ T cell dysfunction was in part reversible upon PD-1 blockade or OX40 costimulation in vitro.

CONCLUSION. Our findings highlight the uniqueness of AML in sculpting CD8+ T cell responses and the plasticity of their signatures upon chemotherapy response, providing a compelling rationale for integration of novel immunotherapies to augment antileukemia immunity.

FUNDING. This work was supported by the Leukemia & Lymphoma Society grant no. 6449-13; NIH grants UM1-CA186691 and R01-HL110907-01; the American Society for Blood and Marrow Transplantation New Investigator Award/Gabrielle's Angel Foundation; the Vienna Fund for Innovative Cancer Research; and by fellowships from the Wenner-Gren Foundation and the Swedish Society for Medical Research.

Introduction

Although up to 70% of newly diagnosed acute myeloid leukemia (AML) patients achieve remission following induction chemotherapy, the majority of them still relapse and die of their disease (1, 2). Much of the work on improving the outcomes in AML has centered on the mechanisms of leukemia cell drug resistance, with little attention given to the effects of chemotherapy in overcoming the inhibitory immune responses in patients who respond to therapy and become long-term survivors. Understanding these immunological effects of chemotherapy in relation to response is highly desirable in order to effectively incorporate strategies aimed at reinstating immunological control of AML (3, 4, 5).

In the leukemia-bearing host, the mechanisms engaged by leukemia cells to regulate immune activation versus tolerance remain underexplored but, in the context of the disseminated nature of this disease, are likely to operate systemically and simultaneously in peripheral blood (PB) and bone marrow (BM). AML is characterized by one of the lowest mutational burdens among different malignancies, suggesting a low immunogenicity; however, the mutational quality rather than quantity may be relevant in eliciting endogenous antileukemia responses (6–8). AML blasts are also endowed with several unique immune evasion mechanisms (9–11), implying their direct role in the creation of the immunosuppressive milieu that inhibits antileukemia immune responses (12, 13). Yet, effector T cells capable of recognizing leukemic cells can be detected in patients with AML (14, 15) and the susceptibility of leukemia to T cell–mediated killing has been demonstrated by the efficacy of allogeneic transplant and donor lymphocyte infusions (DLIs) in this disease (16, 17). Chemotherapy as a frontline treatment of AML also modulates T cell function (18, 19), and robust lymphocyte recovery after treatment is predictive of reduced relapse risk (20).

General understanding of the T cell function in AML at diagnosis and how it is modulated by chemotherapy is still lacking. Gene expression profiling of PB CD8$^+$ T cells in AML patients at diagnosis identified an aberrant activation profile and alterations in genes important for immunologic synapse formation (21). Studies in murine models of AML have shown that the frequency of CD8$^+$ T cells coexpressing inhibitory receptors (IRs) increases with disease progression and that the cytotoxic function can be reinvigorated by checkpoint blockade or genetic ablation resulting in augmented antileukemia immunity (22, 23). Several smaller studies have also shown that CD8$^+$ T cells expressing IRs are functionally impaired and predictive of AML relapse (24–27). Rapid upregulation of immune response–driven resistance mechanisms by primary AML cells that may limit AML elimination has been observed upon in vitro treatment with novel immunotherapeutics that activate T cells (28, 29). Thus, functional T cell exhaustion appears to be operational in AML. In addition to exhaustion, the dysfunctional state of CD8$^+$ T cells encompasses senescence as an intertwined but still mechanistically distinct process that has not been studied in AML (30–33). Further understanding of these phenomena and their relationship to chemotherapy effect is critical to the rational integration of immune therapies in this disease.

In this study, we used a systems immunology approach to interrogate paired patient samples collected at diagnosis and at recovery following induction chemotherapy to decipher the mechanisms of CD8$^+$ T cell dysfunction in AML. Our data support the concept that chemotherapy unleashes the generation of CD8$^+$ immune reactivity that is entwined with achieving clinical response, suggesting that further immune intervention to augment antileukemia reactivity may be of benefit in overcoming the immunological barriers to response in nonresponders to chemotherapy and to maintain an antileukemic milieu in responders.

Results

CD8$^+$ T cells from AML patients exhibit features of exhaustion and senescence but retain capacity to secrete cytokines. Although CD8$^+$ T cells from AML patients have been found to express co-IRs (24–27), this is not sufficient to define them as dysfunctional since co-IRs can also be upregulated during a productive T cell response (34). We first performed immunophenotypic analyses of circulating CD8$^+$ T cells from newly diagnosed AML patients (*n* = 20) to define their state of differentiation, activation, and coinhibitory molecule expression compared with healthy controls (HCs) (*n* = 18). We used CD45RA, CCR7, and CD27 to distinguish between several maturation states of CD8$^+$ T cells (refs. 35, 36, and Supplemental Figure 1A; supplemental material available online with this article; https://doi.org/10.1172/jci.insight.120974DS1), and found a significantly increased percentage of terminally differentiated effector cells (Temra) (CCR7$^-$CD45RA$^+$) and Temra-like cells (CD27$^-$CD45RA$^+$), and a reduced percentage of naive (CCR7$^+$CD45RA$^+$) and naive-like cells (CD27$^+$CD45RA$^+$) in AML patients relative to HCs (Figure 1A). Temra and Temra-like represent analogous populations characterized by heterogeneity, but also enrichment for antigen-experienced and senescent T cells (30, 36, 37). Further characterization revealed a significantly lower percentage of CD8$^+$ T cells expressing CD27, CD28, or CD127 in AML, and a higher percentage of CD8$^+$CD27$^-$CD28$^-$ T cells (*P* < 0.001) (Figure 1B) with end-stage differentiation and senescence properties (38). A higher percentage of AML CD8$^+$ T cells also expressed CD57 (*P* < 0.001), a specific marker of cellular senescence, as well as exhaustion markers 2B4 and PD-1 (both *P* < 0.0001) (Figure 1C and refs. 37–40). The cumulative frequency of CD8$^+$ T cells expressing 1, 2, or 3 markers (CD57, 2B4, or PD-1) was also significantly higher in AML than HCs (*P* = 0.0002) (Figure 1D).
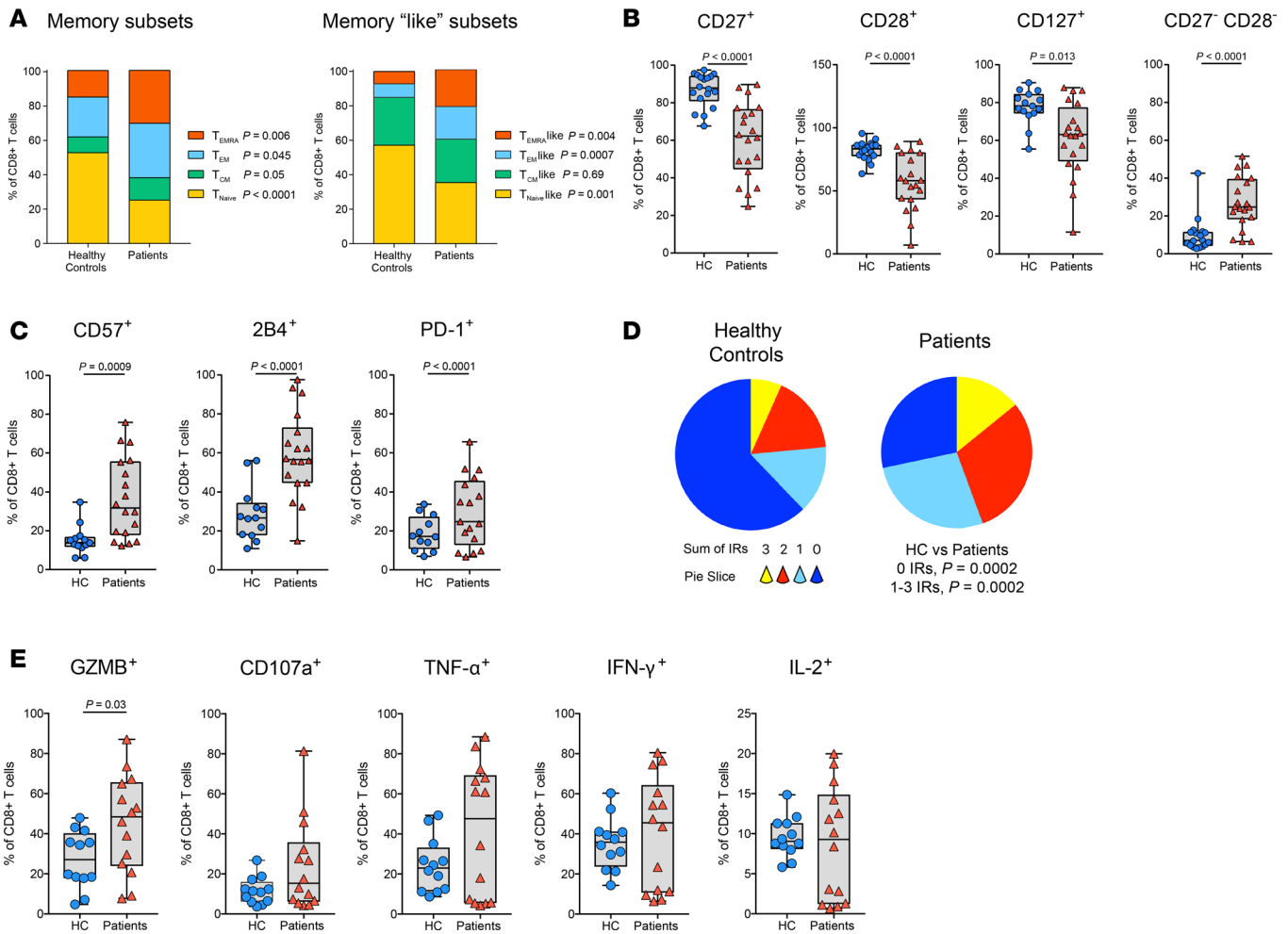
Figure 1. CD8+ T cells from AML patients display phenotypical features of exhaustion and senescence, but are able to secrete cytokines. Pretreatment PB T cells from newly diagnosed AML patients (*n* = 20) and healthy controls (HCs) (*n* = 18) were analyzed by multiparameter flow cytometry. *P* values were calculated using Mann–Whitney *U* test (**A**–**E**). (**A**) CD8+ T cell subsets according to CD45RA and CCR7 (left), and CD45RA and CD27 (right). (**B** and **C**) Expression of (**B**) stimulatory receptors, and (**C**) the senescence marker CD57, and IRs (2B4, PD-1) on CD8+ T cells. (**D**) Boolean gating analysis of the coexpression of PD-1, CD57, and 2B4 on PB CD8+ T cells. Pie slices represent the number of coexpressed markers (0–3) analyzed with SPICE software. (**E**) Expression of effector molecules and cytokines on CD8+ T cells.

To functionally characterize CD8+ T cells from newly diagnosed AML patients, we assessed their cytotoxic molecule expression and cytokine production upon phorbol myristate acetate (PMA)/ionomycin in vitro stimulation. We found that percentages of CD8+ T cells expressing granzyme B (GZMB) were higher in patients (*P* = 0.03), but those expressing CD107a and the cytokines, tumor necrosis factor α (TNF-α), interferon γ (IFN-γ), and interleukin 2 (IL-2) were similar for AML patients and HCs (Figure 1E). Given that cytokine expression by AML CD8+ T cells exhibited a bimodal distribution, likely reflecting different degrees of T cell dysfunction (41), we next measured the median fluorescence intensity (MFI) of cytokine expression. The intensity of TNF-α expression was significantly higher, while IFN-γ trended towards higher expression in AML compared with HCs (Supplemental Figure 1B). In contrast, the intensity of IL-2 expression was significantly lower in CD8+ T cells of AML patients, suggestive of their dysfunction.

Coexistence of senescence and exhaustion phenotypic signatures in AML CD8+ T cells. We next used the viSNE clustering and visualization strategy to examine the expression of PD-1, CD57, and CD45RA together with GZMB, CD107a, and cytokines (TNF-α, IFN-γ, and IL-2) (Figure 2, A and B). The advantage of this analysis lies in its integration of surface and functional markers at a single-cell level, providing an improved understanding of their high-dimensional relationship (42). A cluster characterized by high PD-1 expression was prominent among the AML CD8+ T cells and minimally expressed cytokines. A cluster characterized by high CD57 and GZMB expression and partially positive for CD45RA, was detected in
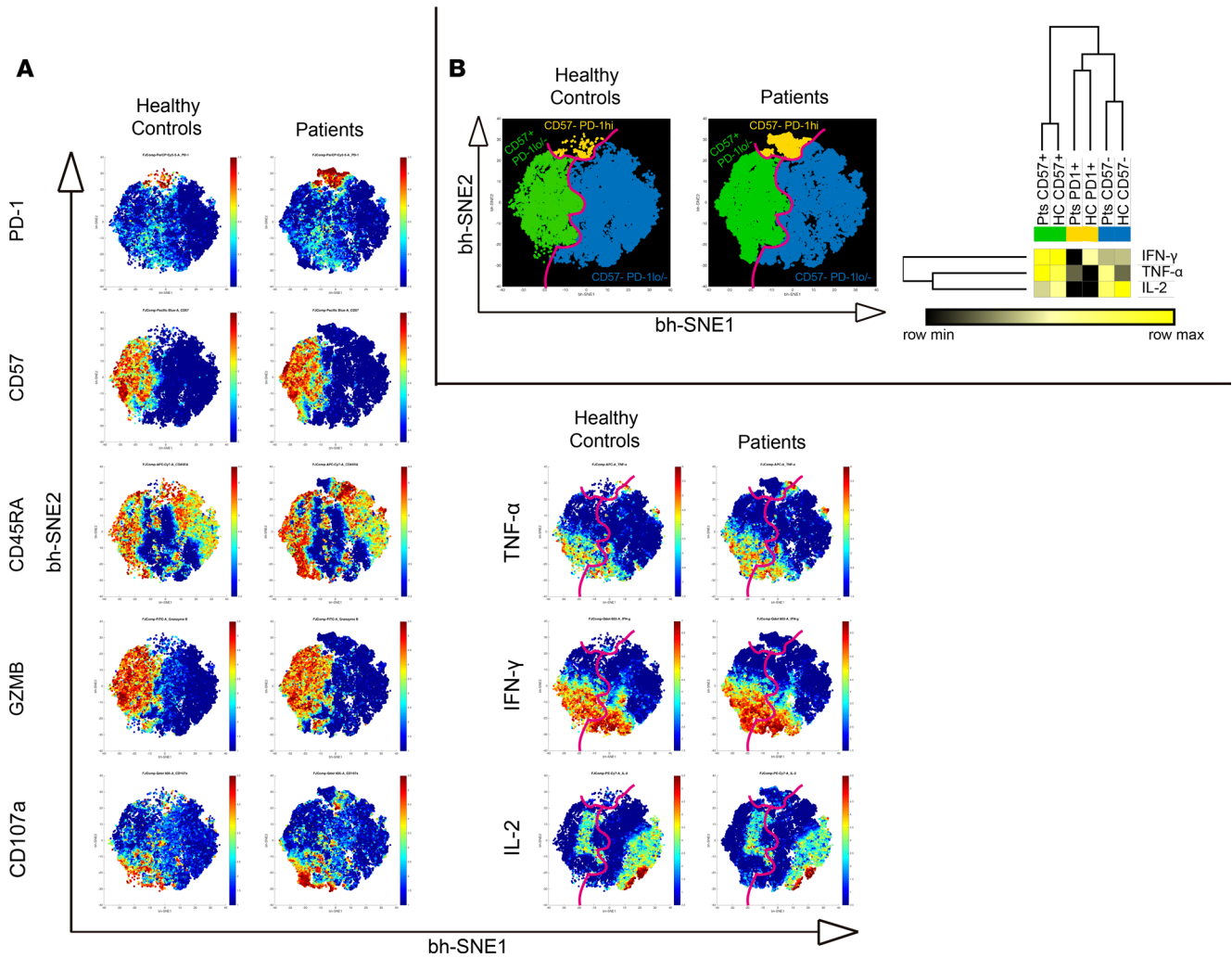
Figure 2. Senescence and exhaustion phenotypes coexist in AML CD8+ T cells. (**A** and **B**) Multidimensional single-cell analysis of PB CD8+ T cells from AML patients before treatment (*n* = 13) and HCs (*n* = 13). (**A**) Bidimensional map obtained from flow cytometric data using the bh-SNE algorithm (pooled data sets). Each point in the map represents an individual cell, and the cells are colored according to the intensity of expression of individual markers, as indicated on the color scale to the right of individual maps. (**B**) Summary map (left) with lines drawn to separate the CD57+ (green), CD57− (blue), and CD57−PD-1hi (yellow) populations. Heatmap (right) represents the percentage of cells in the CD8+CD57+, CD8+CD57−, and CD8+PD-1hi clusters that express IFN-γ, TNF-α, and IL-2, for AML patients and HCs. Clustering analysis and heatmap were generated using Morpheus software.

both AML and HC CD8+ T cells. As cells within both the CD57+ and CD57− cluster expressed cytokines, we next characterized their individual cytokine profile. Using unsupervised clustering we summarized the data in a heatmap (Figure 2B) and also examined MFI of cytokine expression (Supplemental Figure 1C), both of which demonstrated that the frequency and intensity of TNF-α and IFN-γ expression were higher on CD8+CD57+ T cells, while IL-2 was lower compared with CD8+CD57− cells in both HC and AML patients. This is consistent with the phenotype of senescent T cells that are metabolically active and abundantly secrete inflammatory cytokines (37, 43). Notably, the intensity of IL-2 expression was also lower within the CD8+CD57− subpopulation in AML compared with HCs, consistent with the finding of lower production of this cytokine by AML CD8+ T cells overall. Next we investigated whether the level of PD-1 expression correlated with effector molecule and cytokine production in the CD57− population (Supplemental Figure 1D) and found that it negatively correlated with GZMB and IFN-γ expression. Overall, these observations suggest that there are 2 cell populations enriched among AML CD8+ T cells: one having a senescent, high proinflammatory cytokine–expressing phenotype (CD8+CD57+PD-1−/lo) and the other having a functional signature of exhaustion (CD8+CD57−PD-1hi/loIL-2lo) (37, 38, 40, 43).

AML blasts alter viability and the dynamics of co-signaling and senescence molecule expression on CD8+ T cells. We hypothesized that in AML patients, both exhaustion and senescence of CD8+ T cells occur because of

chronic CD8^{+} T cell activation. This prompted us to examine the behavior of AML CD8^{+} T cells upon optimal stimulation and the direct effect of leukemia blast–T cell interactions that occur in the local milieu on T cell function. For these experiments, T cells from newly diagnosed AML patients and HCs were FACS isolated, stimulated with anti–CD3/CD28 beads, and analyzed for viability, proliferation, and expression of co-IRs and costimulatory molecules. This experimental model has been well characterized in relation to the expression pattern of co-signaling molecules on healthy T cells (34). On day +3 after stimulation, the viability and Ki67 expression did not differ between AML and HC T cells (Figure 3A). Both co-IRs (PD-1 and CTLA-4) and costimulatory receptors (OX40 and ICOS) were upregulated on day +3 on AML and HC CD8^{+} T cells compared with baseline expression (Supplemental Figure 2A), except for 2B4 which was downregulated, as reported previously (34). The only significant difference on day +3 was persistently higher expression of 2B4 and CD57 on CD8^{+} T cells from AML patients compared with HCs (Figure 3A). Addition of IL-2 to the cultures (50 IU/ml) significantly increased Ki67 expression of HC CD8^{+} T cells ($P < 0.001$) but had less effect on AML CD8^{+} T cells (Figure 3B). IL-2 addition significantly decreased 2B4^{+} expression in cultures from both HCs and AML patients, and CD57^{+} expression in HC CD8^{+} T cells. Enumeration of the total number of T cells revealed that the fold expansion of AML T cells on day +6 was lower in comparison with HC T cells (Supplemental Figure 2B), likely reflecting an inability of IL-2 to rescue proliferation of senescent CD57^{+} T cells (Figure 3B).

Next, we examined the effect of autologous AML blasts (allogeneic for HC) as an extrinsic modifier of the T cell responses. Coculturing stimulated T cells with FACS-isolated AML blasts resulted in a significantly reduced viability of both AML and HC CD8^{+} T cells on day +3 (Figure 3C). This was also reflected in significantly higher percentages of AML CD8^{+} T cells expressing cleaved caspase-3 upon coculture with blasts compared with T cells cultured and stimulated without blasts ($P < 0.005$) (Supplemental Figure 2C). Coculture of HC CD8^{+} T cells with blasts did not significantly increase the percentage of cleaved caspase-3^{+} cells but more prominently induced their CD57 and 2B4 expression ($P < 0.001$ and $P = 0.01$, respectively) (Figure 3C). These findings are in line with previous observations of increased CD57 expression on T cells in the hematologic malignancies milieu (44, 45) and increased susceptibility to apoptosis of CD8^{+}CD57^{+} cells upon activation or antigen stimulation (46, 47).

We then used cluster identification, characterization, and regression (CITRUS) analysis to independently and in an unsupervised fashion validate whether CD8^{+} populations significantly differed between the groups (HC versus AML, with or without blasts). CITRUS analysis identified CD8^{+}CD57^{+} T cells as a key cluster present in a significantly higher abundance (false discovery rate [FDR] < 0.05) in stimulated AML CD8^{+} T cells cultured alone or with blasts in comparison with HC T cells cultured with or without blasts ($P = 0.0002$) (Figure 3D). The analysis also confirmed that the presence of blasts increased CD57 expression on HC CD8^{+} T cells ($P = 0.03$). The CD57^{+} cell cluster was characterized by low expression of Ki67 (Figure 3D).

Most of the observed PD-1 and CTLA-4 upregulation on CD8^{+} T cells on day +3 after stimulation occurred on CD57^{−} but not CD57^{+} cells in both HCs and AML patients (Supplemental Figure 2D). Further examination of co-signaling molecule expression patterns revealed that coculture of stimulated AML CD8^{+} T cells with blasts resulted in a lesser increase in expression of CTLA-4 ($P = 0.01$), OX40 ($P = 0.003$), and ICOS ($P = 0.08$) on day +3 (Figure 3C and Supplemental Figure 2A) compared with stimulated T cells cultured without blasts. A similar finding was also observed for OX-40 upon coculture of HC CD8^{+} T cells with AML blasts ($P = 0.01$) compared with stimulated HC T cells alone. Comparable impact of blasts on CTLA-4, OX40, and ICOS expression was also noted upon coculture of T cells collected from patients ($n = 3$) at the time of documented complete remission (CR) with autologous blasts obtained at diagnosis versus stimulated CR T cells alone (Supplemental Figure 2E). Multidimensional single-cell analysis using the bh-SNE algorithm identified populations with altered expression of OX40 and ICOS in the presence of the blasts, as depicted in the bh-SNE plot and MFI heatmap (Figure 3E). These findings suggest that direct exposure to leukemia blasts may result in altered co-signaling molecule expression that could be critical for T cell activation.

We next investigated whether blocking PD-1 or stimulating OX40 could influence the expansion potential of AML T cells. With addition of OX40 ligand, sorted AML and HC T cells that were cultured in the presence of blasts displayed a significantly higher in vitro expansion on day +6 ($P < 0.001$ and $P = 0.01$, respectively) (Figure 3F). Addition of anti-PD1 monoclonal antibody (mAb) augmented expansion of AML ($P < 0.001$), but not HC T cells, which could be in part due to higher PD-1 expression on AML CD8^{+} T cells
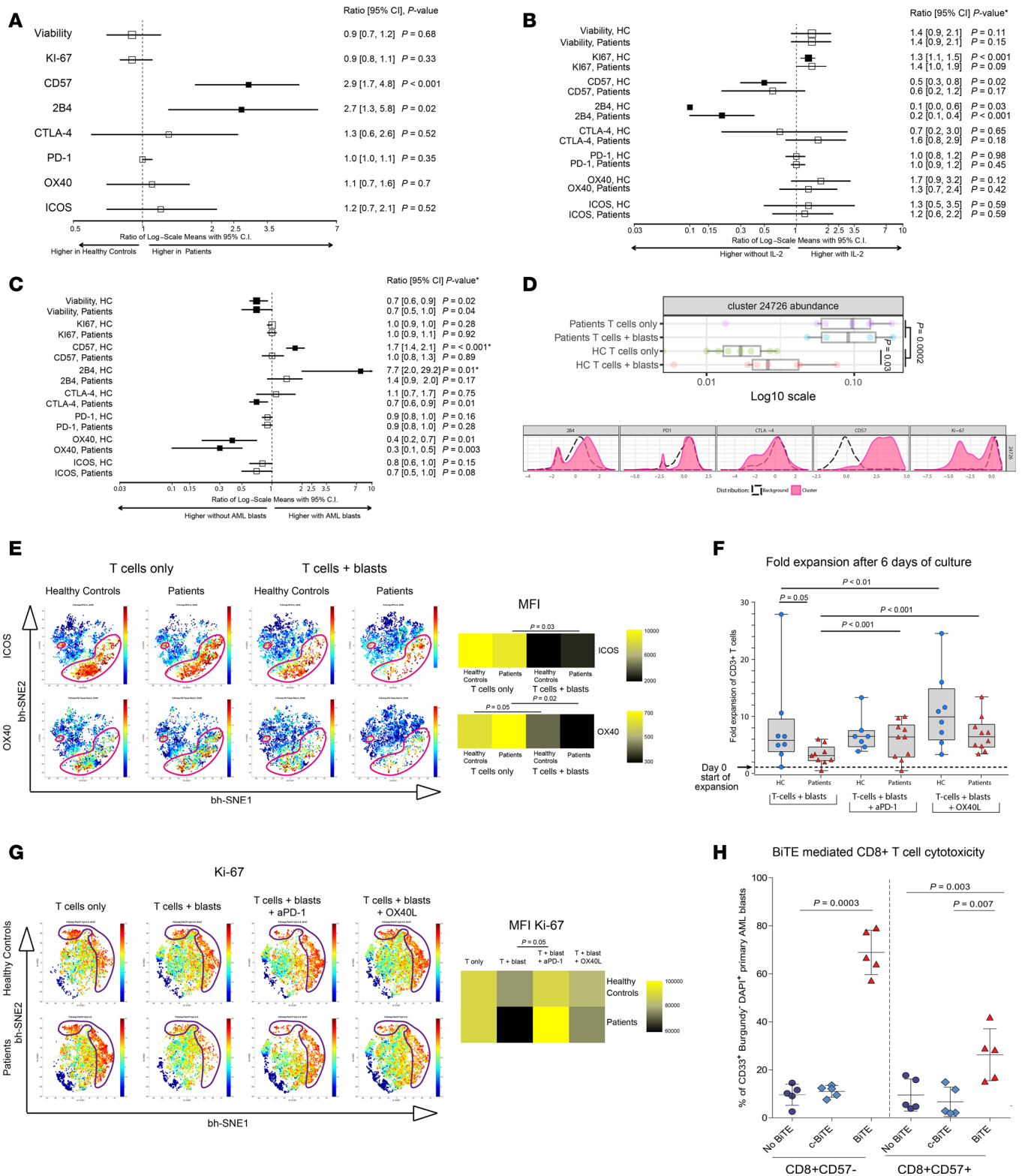
Figure 3. AML blasts alter viability and the expression of co-signaling molecules on CD8+ T cells. Sorted PB T cells from AML patients (n = 20) and HCs (n = 18) were stimulated with anti–CD3/CD28 beads alone or with IL-2 (50 IU/ml) for 3 days. Stimulated T cells were either cultured alone or with autologous blasts (T cells + blasts; allogeneic blasts for HCs) in a 1:10 T cell/blast ratio. (**A**–**C**) Forest plots represent the ratio of log-scale mean percentages of CD8+ T cells expressing each marker as assessed by flow cytometry on day +3, comparing (**A**) AML patients to HCs, (**B**) CD8+ T cells cultured with or without IL-2, and (**C**) CD8+ T cells cultured with or without blasts. *P* values for the ratios being different from 1.0 are shown to the right and were calculated using (**A**) standard and (**B** and **C**) mixed-effects linear regression models. *P < 0.05 for the effect of (**B**) IL-2 and (**C**) blasts between the AML patients and HC. (**D**) CITRUS analysis of flow cytometry data on day +3 for AML patients and HCs. Depicted are cell abundances in clusters identified by CITRUS, stratified by the presence or absence of blasts. *P* values were calculated using Mann–Whitney *U* or Wilcoxon's signed-rank test as appropriate. (**E**) bh-SNE map of

PB CD8+ T cells expressing ICOS and OX40 upon 3-day stimulation in the presence or absence of blasts, both for HCs and AML patients. Each point in the bh-SNE map represents an individual cell, and the cells are colored according to the intensity of expression of the individual marker as indicated on the color scale. CIMminer software was used to summarize the MFI of ICOS and OX40 expression in heatmaps. *P* values were calculated using paired *t* test. (**F**) Fold expansion of AML (*n* = 10) and HC (*n* = 8) CD3+ T cells on day +6 upon culture with blasts and stimulation with anti–PD-1 mAb and OX40 ligand. Dashed horizontal line represents cell count on day 0. *P* values were calculated using mixed-effects linear regression model for the log-scale fold induction as a function of cell source (AML patients and HCs) and stimulator. (**G**) bh-SNE maps of Ki67 distribution on stimulated HC and AML PB CD8+ T cells upon culture alone, or with blasts ± anti–PD-1 mAb or ± OX40 ligand. The heatmap summarizes MFI of Ki67 expression. (**H**) Anti-CD33/CD3 BiTE–mediated cyto-toxicity of CD8+CD57+ or CD8+CD57- T cells towards primary AML blasts (E/T ratio 1:1). Primary patient samples (*n* = 5) were cultured with BiTE or control BiTE (c-BiTE) for 48 hours. Experiments were run in duplicate and *P* values were calculated using paired *t* test.

at baseline. We also examined changes in Ki67 expression by CD8+ T cells as a marker of cellular prolifera-tion and T cell reinvigoration upon checkpoint blockade, as reported previously (48, 49). The bidimensional map on Ki67 expression (Figure 3G) using the bh-SNE algorithm shows that the presence of blasts reduced the intensity of Ki67 expression in AML CD8+ T cells but had less effect on HC T cells. This effect was, in part, reversed by stimulating OX40 or more prominently by blocking PD-1 (*P* = 0.05) on AML T cells.

Lastly, to evaluate the function of PB CD8+CD57- and CD8+CD57+ subpopulations, we examined their abilities to mediate cytotoxicity against autologous CD33+ AML blasts when activated using the anti–CD33/CD3 bispecific T cell–engaging (BiTE) antibody construct. The cytotoxic effect against CD33+ blasts was mediated primarily by the CD8+CD57- subpopulation, while in contrast, the CD8+CD57+ sub-population exhibited limited cytotoxicity (*P* = 0.003) (Figure 3H).

Transcriptional profiles of AML CD8+ T cells differ from that of healthy T cells. To gain further insights into the mechanisms of leukemia-induced CD8+ T cell dysfunction, we next compared transcriptional profiles of highly purified (≥98%) PB CD8+ T cells from newly diagnosed AML patients to age- and CMV-matched HCs. We used the Human Prime View Gene Expression Array (Affymetrix) and selected top differentially expressed genes (DEGs) based on a fold change (FC) of greater than 2 between AML patients and HCs. Using *P* < 0.01 (and FDR < 0.1), we identified a total of 454 (95 by FDR) DEGs, of which 237 (52 by FDR) were upregulated and 217 (43 by FDR) downregulated in AML versus HC CD8+ T cells (Figure 4A and Supplemental Table 1).

In-depth analysis revealed alterations in multiple genes encoding co-signaling molecules that regulate immune responses. We observed overexpression of IR genes *CD244* (encoding 2B4), *CD160*, and those with less-well-characterized inhibitory capacity, *LILRB1* (50) and *CD300A* (51), as well as downregulation of costimulatory receptor genes *CD40LG* and *CD28* in pretreatment AML CD8+ T cells, as shown in the heat-map of selected genes (Figure 4B). IR genes such as *LAG3*, *TIGIT*, and *PVRIG* were also upregulated in AML CD8+ T cells, while stimulatory genes such as *ICOS*, *TNFSF8* (encoding CD30L), *TMIGD2* (encod-ing CD28H), and *TNFRSF25* were downregulated at *P* < 0.05 (Figure 4B).

Pretreatment AML CD8+ T cells were also enriched for gene transcripts associated with effector CD8+ T cell differentiation, such as *IFNG* and *GZMA/GZMB/GZMH*, and the transcription factor genes *EOMES*, *TBX21* (encoding T-bet) (31, 32), and *BATF*, which have been linked to an exhausted CD8+ T cell phenotype (52). Consistent with effector T cell differentiation, we also observed decreased expression of the chemokine *CCR7*.

Among the top upregulated genes in AML CD8+ T cells were also those previously reported to be expressed on senescent T cells such as multiple killer lectin-like and killer cell immunoglobulin-like receptor genes, including *KLRF1*, *KLRC1*, *KIR2DS1*, *KLRD1*, *KLRC3*, *KLRAP1* (53–55), as well as *KLRG1*, *B3GAT1* (encoding CD57), *CCL4* and *CXCR31* (39, 56, 57). In addition, genes involved in apop-tosis, *CASP1* and *FASLG*, as previously described for senescent and exhausted T cells, were upregulated (Figure 4B and ref. 58). In contrast, genes that are involved in T cell adhesion and migration, *ACTN1*, *ALCAM*, and *CKAP2*, were downregulated, in line with the finding by Le Dieu et al. (21) that pretreat-ment T cells of AML patients lacked expression of adhesion molecules.

We validated the microarray data by quantitative real-time PCR (qPCR) of 7 selected genes using PB samples (Supplemental Figure 3A). Without exception, the qPCR gene expression mirrored the findings in the microarray, with *CD28*, *CCR7*, and *CD40LG* being 1- to 2-fold downregulated, whereas *EOMES*, *KLRG1*, *TBX21*, and *GZMB* were 2- to 5-fold upregulated in AML relative to HC. Further, the microarray data are also consistent with protein expression observed by flow cytometry studies for 6 markers (CD28, CD57, 2B4, and GZMB in Figure 1, and T-bet and EOMES in Supplemental Figure 3B).
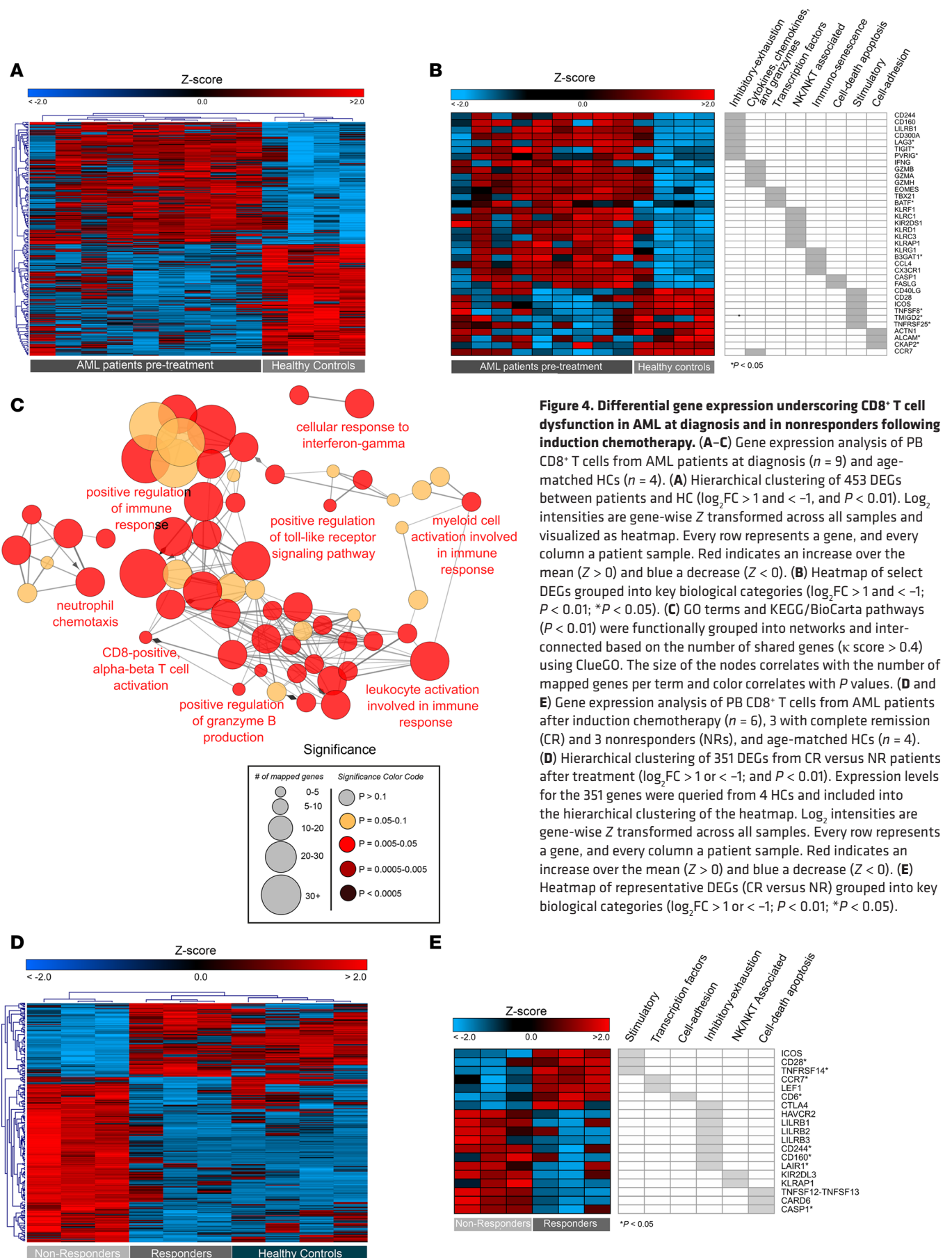
Figure 4. Differential gene expression underscoring CD8+ T cell dysfunction in AML at diagnosis and in nonresponders following induction chemotherapy. (A–C) Gene expression analysis of PB CD8+ T cells from AML patients at diagnosis ($n = 9$) and age-matched HCs ($n = 4$). (A) Hierarchical clustering of 453 DEGs between patients and HC ($\log_2$FC > 1 and < –1, and $P < 0.01$). $\log_2$ intensities are gene-wise Z transformed across all samples and visualized as heatmap. Every row represents a gene, and every column a patient sample. Red indicates an increase over the mean ($Z > 0$) and blue a decrease ($Z < 0$). (B) Heatmap of select DEGs grouped into key biological categories ($\log_2$FC > 1 and < –1; $P < 0.01$; *$P < 0.05$). (C) GO terms and KEGG/BioCarta pathways ($P < 0.01$) were functionally grouped into networks and interconnected based on the number of shared genes (κ score > 0.4) using ClueGO. The size of the nodes correlates with the number of mapped genes per term and color correlates with P values. (D and E) Gene expression analysis of PB CD8+ T cells from AML patients after induction chemotherapy ($n = 6$), 3 with complete remission (CR) and 3 nonresponders (NRs), and age-matched HCs ($n = 4$). (D) Hierarchical clustering of 351 DEGs from CR versus NR patients after treatment ($\log_2$FC > 1 or < –1; and $P < 0.01$). Expression levels for the 351 genes were queried from 4 HCs and included into the hierarchical clustering of the heatmap. $\log_2$ intensities are gene-wise Z transformed across all samples. Every row represents a gene, and every column a patient sample. Red indicates an increase over the mean ($Z > 0$) and blue a decrease ($Z < 0$). (E) Heatmap of representative DEGs (CR versus NR) grouped into key biological categories ($\log_2$FC > 1 or < –1; $P < 0.01$; *$P < 0.05$).

Table 1. Changes in expression of select genes between pre- and posttreatment and according to response

GENE	Postinduction CR vs. Pretreatment NR			
	CR		NR	
	Log$_2$FC	Direction	Log$_2$FC	Direction
ICOS	1.63	↑	−1.77	↓
CD28	1.56	↑	0.50	↔
TNFRSF14	−0.36	↔	−0.44	↔
CCR7	1.29	↑	−0.12	↔
LEF1	1.88	↑	0.37	↔
CD6	1.26	↑	−0.27	↔
CTLA4	1.43	↑	−1.54	↓
HAVCR2	0.59	↔	1.95	↑
LILRB1	−1.82	↓	1.02	↑
LILRB3	0.69	↔	3.77	↑
LILRB2	2.24	↑	6.78	↑
CD244	−1.53	↓	−0.32	↔
CD160	−2.60	↓	−0.77	↔
LAIR1	1.70	↑	1.02	↑
KIR2DL3	0.09	↔	−0.26	↔
KLRAP1	−2.08	↓	−1.04	↓
TNFSF12-TNFSF13	0.50	↔	2.11	↑
CARD6	−0.89	↔	3.26	↑
CASP1	−1.28	↓	1.44	↑

Select genes as shown in Figure 3E, were compared between paired pre- and posttreatment specimens separately for CR and NR patients. ↑ indicates a significant increase from pre- to posttreatment ($P < 0.05$), ↓ indicates a significant decrease ($P < 0.05$), and ↔ indicates no change ($P > 0.05$).

Finally, we investigated whether specific pathways were enriched among DEGs using Gene Ontology (GO) terms compared to a background list including all genes (Supplemental Figure 3C). Pathways associated with immune-related functions were up to 5.74-fold enriched, which was also confirmed by GO network analysis of DEGs using ClueGo (59), a Cytoscape plug-in that creates a functionally organized network of GO, KEGG, and BioCarta pathway terms (Figure 4C).

Response to induction chemotherapy is associated with reversal in the transcriptional profile of AML CD8$^+$ T cells toward one observed in healthy T cells. Given the importance of AML blasts in influencing T cell responses, we hypothesized that a change in the leukemia burden and hematopoietic milieu, induced in response to chemotherapy, could affect the net CD8$^+$ T cell state. Toward that end, we examined and compared the transcriptional profiles of PB AML CD8$^+$ T cells from patients who achieved CR versus those who did not achieve CR (nonresponders, NRs) longitudinally, at pretreatment and upon recovery following induction chemotherapy (paired samples).

The comparison of pretreatment CD8$^+$ T cell transcriptional profiles from AML patients according to their subsequent response to induction chemotherapy (CR versus NR) did not identify significant differences in the expression of immune-related genes at baseline (Supplemental Table 2). In contrast, we observed significant differences in the immune-related gene expression by CD8$^+$ T cells between CR and NR patients after treatment. Using the same significance criteria as above, we identified a total of 351 DEGs; 108 were upregulated and 243 downregulated in CR relative to NR patients (Figure 4D and Supplemental Table 3). We applied the same gene set to HCs and found that expression profiles of CR patients clustered together with those of HCs and were distinct from expression profiles of NR patients, suggesting that the response to chemotherapy is associated with the reversion of CD8$^+$ T cell gene expression profiles toward a healthy-like pattern. In contrast, NR patients' CD8$^+$ T cell gene expression profiles did not evince reversion to a normal pattern.

In-depth analysis of the selected gene set (Figure 4E) revealed that the immune stimulatory receptor genes *ICOS*, *CD28*, and *TNFRSF14* (encoding HVEM) had significantly higher expression in CD8$^+$ T cells from CR patients relative to NR patients, while IRs, including *HAVCR2* (encoding TIM3), CD244, CD160,

several members of the inhibitory *LIR* receptor family, and *LAIR1* (60) had significantly lower expression. Interestingly, *CTLA4* expression was also higher in CR patients, following the same trend observed with *CD28* and other stimulatory genes, leading us to hypothesize that *CTLA4* upregulation is likely in response to T cell activation. Furthermore, 2 KIR-associated receptor genes (*KIR2DL3*, *KLRAP1*) (53–55), as well as genes involved in T cell apoptosis, including *TNFSF12-TNFSF13* (TWEAK-APRIL), *CARD6* (caspase recruitment), and *CASP1* (58, 60) were significantly less expressed in CR versus NR CD8+ T cells. In contrast, *CCR7*, *LEF1*, which represses Foxp3 and RORC expression in CD8+ T cells (61), and *CD6* (62), which plays a role in immune synapse formation, were all more highly expressed in CR CD8+ T cells.

We also examined the direction of change of selected DEGs by comparing their posttreatment to pretreatment expression according to response (Table 1). In general, the differences in gene expression between CD8+ T cells of CR versus NR patients after treatment were predominantly due to upregulation of costimulatory (*ICOS*, *CD28*), transcription factor and cell adhesion genes (*LEF1*, *CCR7*, *CD6*), with concomitant downregulation of coinhibitory genes (*CD244*, *CD160*) in CR CD8+ T cells. In contrast, upregulation of coinhibitory genes (*HAVCR2*, *LIR* receptor family) and genes involved in apoptosis was detected in NR CD8+ T cells. The expression of *ICOS* and *CTLA4* changed in opposite direction in relation to response, becoming upregulated in CR and downregulated in NR CD8+ T cells. These gene expression changes are consistent with flow cytometry changes of select markers expression in relation to response (CD28 and CTLA-4 in Supplemental Figure 3D).

We next examined the top enriched GO terms for the DEGs (Supplemental Figure 3, E and F) and found up to a 9.86-fold enrichment of GO terms associated with immune-related functions.

Response to treatment is associated with the activation of costimulatory signaling pathways and enrichment in gene sets associated with effective CD8+ T cell responses. To define additional transcriptional signatures and biological pathways associated with CD8+ T cell dysfunction in AML and their changes in relation to response after chemotherapy, we applied computational approaches to extract biological meanings from the sets of DEGs identified above. We first conducted gene set enrichment analysis (GSEA) using published gene sets from landmark studies characterizing human CD8+ T cell differentiation (63), PD-1 expression (64), and exhaustion in chronic viral infections and cancer (52), as well as curated gene sets from the Molecular Signatures Database (MsigDB). For analysis of T cell differentiation (63), we used expression data from ArrayExpress (E-TABM-40) and derived unique gene modules for each of the naive, central memory (Tcm), effector memory (Tem), and Temra subsets (Supplemental Figure 4A and Supplemental Table 4A). The relative enrichment (normalized enrichment score, NES) from GSEA using the obtained distinct immune signatures was visualized as Windmill plots (Figure 5, A and B). We found that the Temra gene set was highly enriched (NES of 3.2) in PB CD8+ T cells from AML patients at diagnosis when compared with HCs (Figure 5A). After induction chemotherapy, a strong enrichment for transcriptional signatures of naive and Tcm cells was found only in CR patients (NES of 2.2 and 1.93, respectively) (Figure 5B).

Probing MSigDB and published gene sets revealed that AML CD8+ T cells at diagnosis were highly enriched for the signatures characteristic of PD-1hi and PD-1lo CCR7– effector cells (Figure 5C). Gene signatures of PD-1hi and PD-1lo CD8+ T cells, characterized in relation to naive cells in healthy human subjects, were found to be representative of effector memory rather than exhausted cells (64). After chemotherapy, we observed strong enrichment in a naive CD8+ T cell gene signature only in CR patients (Figure 5D). To examine whether AML CD8+ T cells have any transcriptional similarity to exhausted cells, we used publicly available gene expression data to derive gene sets of HIV-specific CD8+ T cells from progressors (those with chronic active disease) and from controllers (those with contained viral loads) (52), and queried our data sets (Supplemental Figure 4B and Supplemental Table 4B). GSEA revealed that AML CD8+ T cells at diagnosis were enriched for the progressor gene set (Figure 5C), consistent with exhausted CD8+ T cells seen in chronic viral infection. Following chemotherapy, CD8+ T cells from CR patients reversed to a gene signature characteristic of controllers, whereas NR patients continued to show enrichment for an exhausted gene signature associated with the progressors (Figure 5D).

AML CD8+ T cells at diagnosis were also enriched for genes expressed by tumor-specific (Melan-A/MART-1) compared to CMV or EBV virus-specific T cells (65), and by CD8+ T cells undergoing deletion (Supplemental Figure 4C and ref. 66), a tolerance mechanism associated with immune dysfunction in AML (11). In addition, the senescence gene signature was enriched in NRs (Supplemental Figure 4D).

Lastly, to identify transcriptional pathways associated with AML CD8+ T cell dysfunction, we applied ingenuity pathway analysis (IPA) to the list of DEGs between pretreatment AML versus HC CD8+ T cells
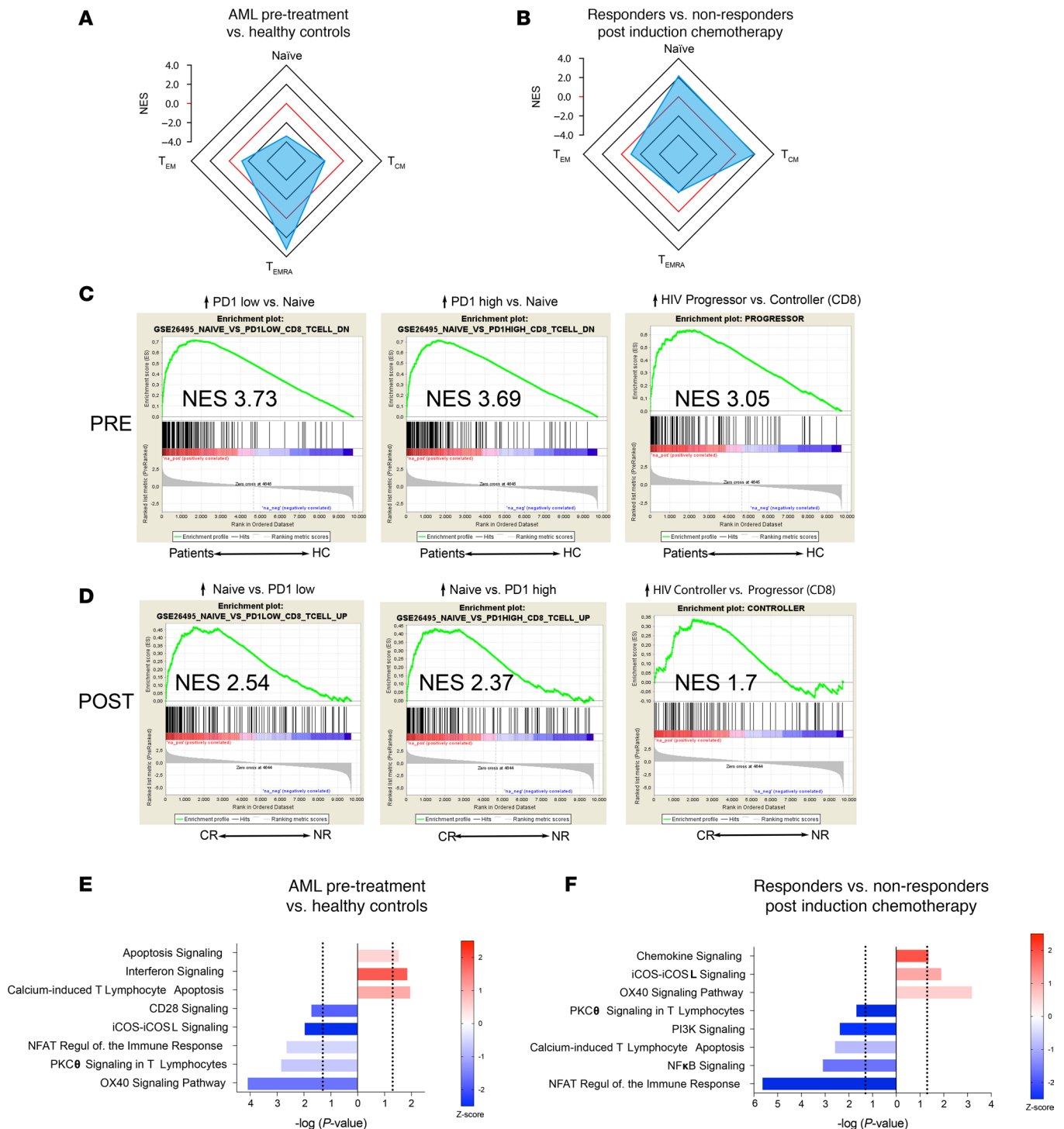
Figure 5. GSEA and biological pathways analysis from the pretreatment and posttreatment comparisons identified unique gene sets and pathways altered in AML CD8+ T cells. (**A** and **B**) Windmill plots showing relative gene set enrichment of public expression data (E-TABM-40) derived gene sets (naive, Tcm, Tem, Temra) (Supplemental Figure 4A) for (**A**) pretreatment AML versus HC and (**B**) posttreatment AML CR versus NR. A normalized enrichment score (NES) of 0.0 is marked red, negative NES increases toward the center, whereas positive NES increases outwards. (**C** and **D**) Summary graphs of representative GSEA enrichment plots of select immune-related gene sets overrepresented in (**C**) pretreatment and (**D**) posttreatment analyses from gene sets derived from the MSigDB (Broad Institute) and custom sets. (**E** and **F**) Ingenuity pathway analysis of the differentially expressed genes ($\log_2$FC > 1 and < −1; $P < 0.05$) for (**E**) pretreatment AML versus HC, and (**F**) posttreatment AML CR versus NR. Pathways were selected according to $P < 0.01$ and availability of a predictive Z score. Activated pathways (positive Z score) are colored red; inhibited pathways (negative Z score) are colored blue.

(Supplemental Table 5). The most prominent finding was activation of T lymphocyte apoptosis and IFN signaling pathways and inhibition of CD28, ICOS, and OX40 signaling pathways in AML CD8+ T cells in comparison with HCs (Figure 5E). When we applied IPA to the DEG set after treatment (Supplemental Table 6 and Figure 5F), the notable difference was activation of costimulatory ICOS and OX40 signaling pathways, and inhibition of the calcium-induced T lymphocyte apoptosis pathway in CD8+ T cells from responding patients compared with NRs.

Exhaustion and senescence marker expression changes with therapeutic response. Prompted by observations in our initial studies and transcriptional changes in PB AML CD8+ T cells following treatment, we extended immunophenotypic studies to both PB and BM CD8+ T cells before and after induction chemotherapy. The clinical details/outcome of 59 patients whose samples were used in analyses are presented in Supplemental Tables 7 and 8. As controls we used PB (*n* = 56) and BM (*n* = 24) specimens from healthy subjects. Because the age distribution of our HC cohort indicated a younger population compared with the patients with AML, we performed a sensitivity analysis by sampling with replacement from our HC cohort to create an age-matched control cohort for the AML patients and compared the results to those obtained using a linear regression approach comparing AML patients to all HCs that included age as a covariate. The sets of results comparing AML patients to age-matched controls and AML patients to all HCs, adjusting for age, did not widely differ within subsets. Accordingly, we included age as a covariate for adjustment in all of our large cohort analyses comparing AML to HCs.

T cell differentiation in PB and BM of newly diagnosed AML patients, examined using CD45RA, CCR7, and CD27, followed the same trend as observed in the initial cohort (Figure 1A) and by others (25), having higher percentages of Temra and Temra-like cells, and decreased percentages of naive and naive-like cells, but it did not reach statistical significance relative to HCs (Supplemental Table 9). At the time of recovery from chemotherapy, the percentages of Temra and Temra-like were significantly higher in PB and BM of NR versus CR patients. We found that PB and BM Temra cells significantly declined only in CR patients compared with pretreatment levels (*P* = 0.008 and *P* = 0.02, respectively), whereas their levels remained higher and unchanged compared with baseline in PB and BM of NR patients, consistent with the pattern seen in our gene expression studies.

Next, we examined the expression of IRs on T cells using 2 flow cytometry panels containing differentiation markers as well as PD-1, CD57, KLRG1, and CD160 (panel 1), and Tim3, 2B4, and BTLA (panel 2). We found that significantly higher percentages of AML PB CD8+ T cells express PD-1, CD160, 2B4, Tim3, KLRG1, and CD57 compared with HCs (Table 2). While similar expression trends for all IRs were also observed in the BM, only the percentage of CD8+ T cells expressing CD160 or CD57 was significantly increased in AML compared with HCs. Following chemotherapy, the percentages of both PB and BM CD8+ T cells expressing KLRG1, CD160, or 2B4 significantly decreased, whereas those expressing Tim3 increased in the PB only. When analyzed by response, we found that these PB and BM changes were mostly restricted to CR patients following chemotherapy. In contrast, NR patients showed an increase in the percentages of cells expressing PD-1, Tim3, and BTLA in the BM compared with their pretreatment levels (*P* = 0.001, *P* = 0.007, and *P* = 0.05, respectively) (Table 2).

Analysis of the simultaneous expression of the IRs included in panel 1 and panel 2 revealed that AML patients at diagnosis had higher percentages of CD8+ T cells coexpressing 2 or 3 IRs in PB (Figure 6, A and B) and less prominently in the BM (Supplemental Figure 5, A and B), compared with HCs. Upon treatment, the IR expression pattern changed significantly in CR compared with NR patients, with the percentage of CD8+ T cells coexpressing 2 or 3 IRs decreasing in the PB and BM of CR patients. Given the limited number of patients having minimal residual disease (MRD) defined either by cytogenetics, flow cytometry, or PCR, we could not assess the impact of MRD on the changes in IR expression in patients who achieved CR.

Impact of patient and disease variables on CD8+ T cell phenotypes. We then examined the effect of disease (cytogenetic risk group, de novo versus secondary AML, European LeukemiaNet [ELN] category [ref. 1], WBC count, percent blast in PB and BM, and absolute PB blast count at presentation) and patient variables (sex, CMV, age) on CD8+ T cell differentiation, expression of IRs and senescence markers at diagnosis. Using linear models we found that only BM CD8+ Tcm-like and BM CD8+ naive cells were affected by WBC count at presentation and AML pathogenesis (de novo versus secondary), respectively, but did not observe any substantial influence of other disease variables on the analyzed immunological phenotypes (Supplemental Figure 6A). CMV serostatus appeared to affect the PB CD8+ Temra-like population, although it did not reach statistical significance. We found that age had limited effect on the frequency of several immunological

Table 2. Statistical comparisons of IR expression on PB and BM CD8⁺ T cells before and after treatment

CD8⁺ T cells	Controls Mean (SD)	AML pretreatment					AML post-induction chemotherapy					Over-time analyses	
		Pre (all) Mean (SD)	Contr. vs. Pre (all) P value	CR Mean (SD)	NR Mean (SD)	CR vs. NR P value	Post (all) Mean (SD)	CR Mean (SD)	NR Mean (SD)	CR vs. NR P value	Post (all) vs. Pre (all) P value	CR Post vs. CR Pre P value	NR Post vs. NR Pre P value
Peripheral Blood													
CD8⁺PD-1⁺	15.8 (8.8)	34.9 (15.8)	**0.003**	35.4 (15.4)	33.2 (18)	ns	35.3 (22)	36.1 (24.3)	32.8 (13.5)	ns	↕ ns	↕ ns	↕ ns
CD8⁺KLRG1⁺	34 (17.4)	50.7 (19.4)	**0.05**	50 (18.2)	52.5 (23)	**0.02**	39.5 (18.3)	34.8 (14.6)	51.5 (21.7)	**0.02**	→ **0.001**	→ **<0.0001**	↕ ns
CD8⁺CD160⁺	7.8 (5.2)	16.6 (10.9)	**0.03**	15.2 (9.2)	20.2 (14.4)	ns	11.2 (11.5)	7.7 (6.5)	19.7 (16.4)	ns	→ **0.0002**	→ **0.0001**	↕ ns
CD8⁺CD57⁺	13.3 (8.4)	32.9 (21.1)	**0.001**	30.9 (19.1)	38.9 (26.3)	ns	30.6 (22.3)	26.5 (22)	40.2 (20.8)	**0.04**	↕ ns	↕ ns	↕ ns
CD8⁺Tim3⁺	17.1 (10.2)	26.6 (14.6)	**0.005**	25.6 (13.9)	29.4 (16.8)	ns	34.3 (16.9)	34.1 (17.9)	34.9 (14.6)	ns	← **0.03**	← **0.05**	↕ ns
CD8⁺2B4⁺	36.3 (24.3)	58 (24)	**0.01**	53.6 (23.5)	68.9 (22.3)	ns	36.5 (23.9)	29.1 (16.9)	53.7 (29.2)	**0.01**	→ **<0.0001**	→ **<0.0001**	→ **0.01**
CD8⁺BTLA⁺	16.2 (12.6)	18.2 (18.3)	ns	16.9 (15.4)	21.4 (24.4)	ns	17.2 (16.5)	15.8 (13.9)	20.6 (21.7)	ns	↕ ns	↕ ns	↕ ns
Bone Marrow													
CD8⁺PD1⁺	39.1 (19.2)	44.9 (14)	ns	48 (12.6)	35.7 (14.7)	**0.01**	48.6 (19.1)	47.1 (21.4)	52.5 (11)	ns	↕ ns	↕ ns	← **0.001**
CD8⁺KLRG1⁺	47.8 (19.9)	51.3 (15.7)	ns	49.7 (14.5)	56.5 (19.4)	ns	44.6 (18.6)	39.6 (15.5)	62.4 (18.8)	**0.009**	→ **0.02**	→ **0.003**	↕ ns
CD8⁺CD160⁺	30.5 (18.2)	23.4 (19.3)	**0.05**	23.5 (19.3)	22.9 (20.3)	ns	17.1 (11.9)	14.6 (7.4)	25.7 (19.7)	ns	→ **0.03**	→ **0.01**	↕ ns
CD8⁺CD57⁺	21.6 (15.8)	29.1 (15.9)	**0.05**	26.7 (13.1)	37.5 (22.2)	ns	33.7 (19.6)	28.7 (19.4)	47.8 (12.2)	**0.009**	↕ ns	↕ ns	↕ ns
CD8⁺Tim3⁺	25.2 (18.8)	26.9 (12.9)	ns	29 (13.7)	19.9 (5.9)	ns	33 (17.8)	32.2 (19.6)	35.6 (11)	ns	↕ ns	↕ ns	← **0.007**
CD8⁺2B4⁺	48.1 (25.6)	65.4 (20.9)	ns	61.5 (18.2)	75.9 (24.8)	ns	51.2 (24.2)	43.9 (19.9)	69.1 (25.3)	**0.03**	→ **0.0003**	→ **0.0002**	→ ns
CD8⁺BTLA⁺	21.4 (15)	26 (22.9)	ns	23.1 (21.9)	34.7 (24.8)	ns	29.8 (25)	21.6 (21)	50 (23.4)	**0.02**	↕ ns	↕ ns	← **0.05**

Presented are pretreatment, posttreatment, and over-time analyses according to response to therapy for 59 paired patient samples, and HC samples (PB, n = 56; BM, n = 24). P values for differences between HCs and AML patients are from linear regression models using logarithmically transformed numbers and adjusted for age. P values for differences between patient groups over time are from mixed-effects linear regression models using logarithmically transformed numbers, adjusted for age and including a random intercept for each patient. For more intuitive comprehension by the reader, values are presented as raw mean percentages (±SD).

phenotypes in both patients and HCs, mainly in PB (proportion of variance, median $R^2 = 0.06$; Supplemental Figure 6B).
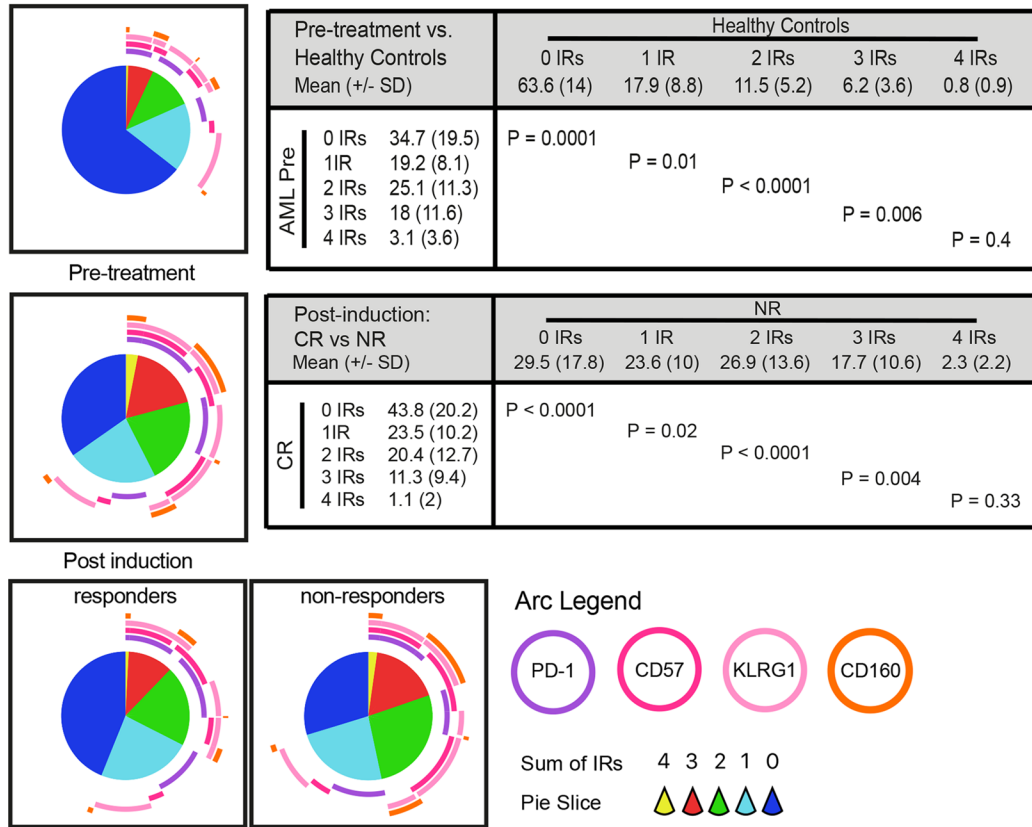
Discussion

There is growing appreciation that certain chemotherapies and targeted agents used for treatment of solid tumors exert their antitumor effect at least in part through immune activation (3). However, little is known about the impact of chemotherapy on immune response in a systemic malignancy such as AML. By examining a sizeable number of primary AML and HC specimens we have identified CD8⁺ T cell dysfunction as an operative immune-escape mechanism in AML patients. Comprehensive immunologic studies on paired pre- and postchemotherapy samples revealed that the transcriptional and phenotypic T cell footprint of response distinguishes responders from NRs to therapy.

T cell dysfunction comprises several differentiation programs of functional unresponsiveness, including T cell exhaustion, anergy, self-tolerance, and senescence (31–33). Several findings support our observations that multiple aspects of deranged T cell function are operative in AML, with senescence and exhaustion being the dominant processes, which clearly differs from observations in solid tumors (67). Both phenotypic and transcriptional studies revealed that CD8⁺ T cells with senescent phenotype are increased at AML diagnosis and persist with increased frequency only in NR patients. These senescent T cells, phenotypically characterized by an increased expression of CD57 and KLRG-1 (30, 38), were found to be a major producer of cytokines with the exception of IL-2. In functional studies, CD8⁺CD57⁺ T cells from AML patients exhibited proliferative arrest that was not rescuable by IL-2, and upon stimulation, in contrast to their CD57⁻ counterparts, did not prominently upregulate co-IRs PD-1 or CTLA-4. More importantly, CD8⁺CD57⁺ T cell cytotoxicity against autologous CD33⁺ blasts upon activation with anti–CD33/CD3 BiTE was limited compared with CD8⁺CD57⁻ T cells, underscoring their functional impairment.

Consistent with murine AML models and several (albeit small) studies of heterogeneous cohorts of AML patients (24–27), we also detected increased IR expression, not only of PD-1, but also coexpression of multiple IRs on CD8⁺ T cells at diagnosis. A higher expression

A Healthy Controls

Pre-treatment

Post induction

responders

non-responders

Pre-treatment vs. Healthy Controls Mean (+/- SD)	Healthy Controls				
	0 IRs 63.6 (14)	1 IR 17.9 (8.8)	2 IRs 11.5 (5.2)	3 IRs 6.2 (3.6)	4 IRs 0.8 (0.9)
AML Pre 0 IRs 34.7 (19.5)	P = 0.0001				
1IR 19.2 (8.1)		P = 0.01			
2 IRs 25.1 (11.3)			P < 0.0001		
3 IRs 18 (11.6)				P = 0.006	
4 IRs 3.1 (3.6)					P = 0.4

Post-induction: CR vs NR Mean (+/- SD)	NR				
	0 IRs 29.5 (17.8)	1 IR 23.6 (10)	2 IRs 26.9 (13.6)	3 IRs 17.7 (10.6)	4 IRs 2.3 (2.2)
CR 0 IRs 43.8 (20.2)	P < 0.0001				
1IR 23.5 (10.2)		P = 0.02			
2 IRs 20.4 (12.7)			P < 0.0001		
3 IRs 11.3 (9.4)				P = 0.004	
4 IRs 1.1 (2)					P = 0.33

Arc Legend

PD-1   CD57   KLRG1   CD160

Sum of IRs   4 3 2 1 0
Pie Slice

B Healthy Controls

Pre-treatment

Post induction

responders

non-responders

Pre-treatment vs. Healthy Controls Mean (+/- SD)	Healthy Controls			
	0 IRs 54.2 (12.3)	1 IR 40.1 (10.7)	2 IRs 5.7 (3.6)	3 IRs 0.1 (0.1)
AML pre 0 IRs 24.7 (12.9)	P = 0.001			
1IR 55.4 (15.4)		P = 0.02		
2 IRs 17.6 (11.8)			P = 0.0002	
3 IRs 2.3 (5.5)				P = 0.04

Post-induction: CR vs NR Mean (+/- SD)	NR			
	0 IRs 26.2 (15)	1 IR 48.6 (15.1)	2 IRs 20.5 (15.8)	3 IRs 4.3 (7.1)
CR 0 IRs 40.8 (17)	P = 0.0002			
1IR 45.3 (12.5)		P = 0.02		
2 IRs 13.5 (8.2)			P < 0.0001	
3 IRs 0.6 (0.8)				P = 0.01

Arc Legend

TIM-3   2B4   BTLA
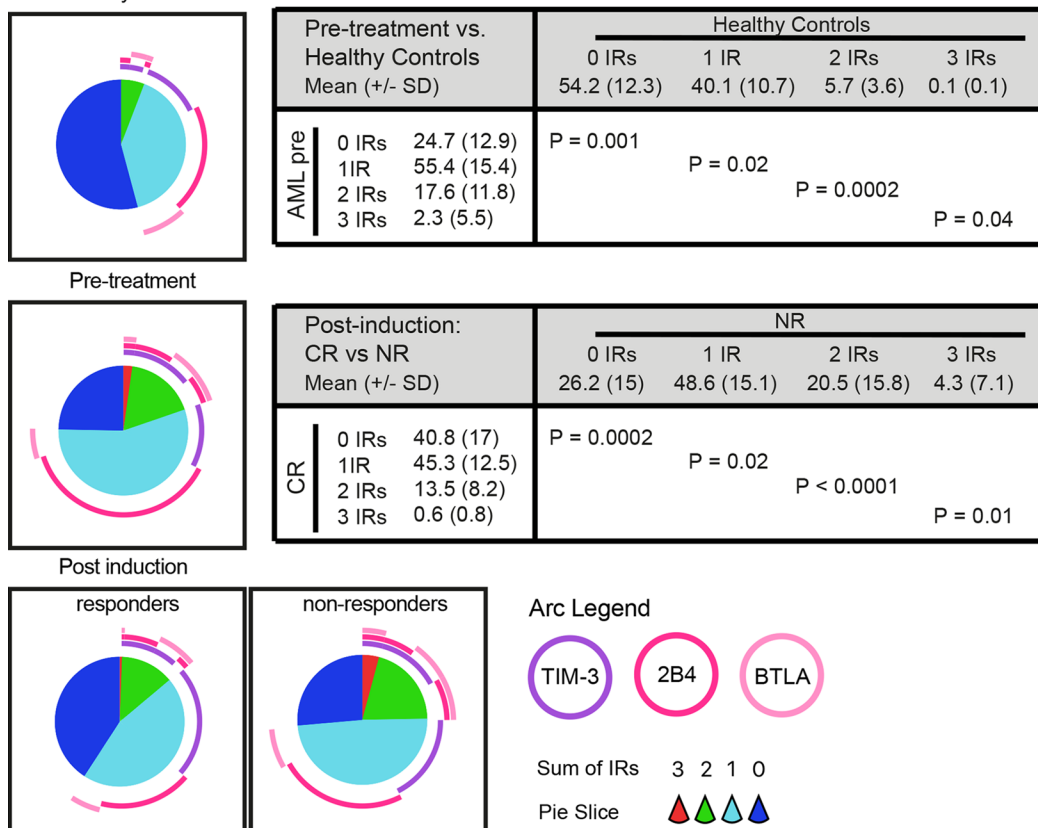
Sum of IRs   3 2 1 0
Pie Slice

Figure 6. CD8+ T cells from AML patients are characterized by coexpression of IRs that change in response to chemotherapy. (**A** and **B**) Immunophenotyping by flow cytometry was performed on paired pre- and posttreatment PB CD8+ T cells. Boolean gating analysis of the coexpression of multiple IRs on PB CD3+CD8+CD56− T cells from AML patients (*n* = 32) and HC (*n* = 21). (**A**) Coexpression of PD-1, CD57, KLRG1, and CD160 (panel 1). (**B**) Coexpression of TIM-3, 2B4, and BTLA (panel 2). Colors of pie slices depict the number of coexpressed IRs (0–3 or 4 IRs), while arcs depict the expression of individual IRs. Coexpression was analyzed with SPICE software. Mean percentages (±SD) of IR coexpression were compared, and corresponding *P* values for the differences between HCs and AML patients before treatment and CR versus NR patients after treatment were calculated using Mann-Whitney *U* test and are shown in tables.

of IRs on AML CD8+ T cells compared with HCs was more apparent in PB than in the BM, in part reflective of a higher baseline IR expression on HC BM versus PB CD8+ T cells. In contrast, the longitudinal changes in the pattern of IR expression were detectable in both PB and BM, and most striking in the BM CD8+ T cells from NR patients that upregulated several exhaustion markers such as PD-1, Tim3, and BTLA, a phenotype characteristic of highly dysfunctional T cells (68). CR patients downregulated several IRs both in PB and BM. Lastly, we also observed that exposure to blasts in vitro promotes apoptosis of CD8+ T cells from AML patients, consistent with recent observations that apoptosis of CD8+ tumor-infiltrating lymphocytes in the tumor microenvironment may be a contributing factor to their inability to reject tumors (69).

Our observations are further supported by gene expression studies, indicating upregulation of multiple genes associated with effector T cell differentiation, as well as T cell exhaustion and senescence in AML CD8+ T cells at diagnosis compared with HCs. Moreover, decreased expression of costimulatory molecules and alteration in genes regulating diverse nonimmune cell survival–related mechanisms including apoptosis, cell signaling, and cell motility further defined the immunological signature of CD8+ T cells in AML. The latter finding is consistent with deregulated expression of genes involved with cytoskeleton and cellular polarization reported by Le Dieu et al. (21). Reversibility of altered CD8+ T cell transcriptional signatures occurred only with response to chemotherapy, which is similar to changes in T cell exhaustion signatures occurring after DLI in CML patients (70).

Moreover, using GSEA, we found that at diagnosis, AML CD8+ T cells share a global gene expression pattern with the exhausted CD8+ T cells in chronic viral infections (52). Following chemotherapy, CD8+ T cells from CR patients reversed to a gene signature characteristic of HIV-specific CD8+ T cells from controllers. In contrast, CD8+ T cells in NRs continued to show enrichment not only for the exhausted gene signature associated with the clinical progressor phenotype, but also for the gene signature of senescent T cells. Interestingly, newly diagnosed patients also shared enrichment for the gene signature characteristic of CD8+ T cells undergoing deletion. This mechanism of peripheral T cell tolerance, previously recognized in a murine model of AML, also seems to be relevant in patients with AML (11).

Several important new findings have emerged from our data. First, T cell dysfunction in AML differs from solid tumors by having more senescent T cells (33, 67), but shares the coexistence of senescence and exhaustion with other systemic hematologic malignancies such as chronic lymphocytic leukemia and myeloma (44, 45, 71). Our data are also consistent with those of Schnorfeil et al. (27) showing that the global cytokine expression by AML CD8+ T cells does not differ from healthy T cells. However, in contrast to healthy CD8+ T cells, the enriched senescent CD8+ T cell population is an important cellular source of cytokines in AML, while remaining CD8+ T cells have a decreased expression of IL-2, indicative of their exhaustion. Second, we show that AML blasts directly affect T cells by promoting their senescence, altering their co-signaling molecule expression, and ultimately impeding their viability in vitro. These effects appear to be susceptible to change upon immune interventions such as PD-1 inhibition or stimulation through OX-40, which lead to improved T cell proliferation and expansion. The reinvigoration of CD8+ T cells in CR patients was also notable for OX40 and ICOS signaling pathway activation, underscoring the importance of the interplay between coinhibitory and costimulatory pathways in defining T cell functionality in the setting of active disease and after treatment. The translational implications of these findings for augmenting antileukemia immunity remain the focus of ongoing investigation. Finally, the overall pattern of IR expression in our study appeared to be independent of specific AML prognostic groups, an observation that requires further examination in a larger number of patients having specific genetic/molecular aberrations.

Our studies have several limitations. First, perhaps because of AML heterogeneity and sample size, our studies did not uncover predictive immune-based biomarkers of response associated either with AML characteristics or the CD8+ T cell subsets detected at baseline. Second, we did not examine how our findings relate to the leukemia-specific immunity due to the complexity in identifying antigen-specific cytotoxic immune cells, but this is a fertile area for future studies. Interestingly, recent studies suggest that surface exposure of calreticulin by AML blasts (72), or the presence of NPM1 mutation (73) may elicit T cell responses that are associated with improved clinical outcomes. However, based on our functional studies, including data on the cytotoxic function of different CD8+ T cell populations (CD57+ versus CD57−), we favor the hypothesis that exhaustion and senescence properties, as seen in CD8+ T cells of AML patients, likely reflect the phenotypic and functional characteristics of both leukemia-specific and bystander T cells that contribute to an overall antileukemia immunity. Finally, a limitation of our study is that the age distribution was greater in the AML

patient cohort than HCs, due to limited availability of older-age healthy donors. To address this we included age as a covariate for adjustment in all of our large cohort analyses comparing AML to HC. Further using linear modeling, we found that age and CMV serostatus, both variables known to have a broad influence on the immune system (74, 75), had limited effect on immune phenotypes in AML.

In summary, our study is the first to our knowledge to provide critical insights into longitudinal changes in CD8+ T cell differentiation, function, and genomic signatures at diagnosis and after treatment in patients with AML. Our in-depth analysis of immunological markers reveals that CD8+ T cells in patients with AML exhibit phenotypic and genotypic features of both exhaustion and senescence. While both processes are encountered in the setting of chronic antigen stimulation, they may be differentially susceptible to therapeutic modulation (30, 37). Recently, immune checkpoint inhibition has been successfully applied in treatment of many solid and some hematologic malignancies. However, not all patients benefit from this approach and extensive efforts are underway to define predictive biomarkers of response to these agents (76). The role of checkpoint inhibition in AML patients has been less-well studied, but several early reports suggest a potential role for CTLA-4 and PD-1 inhibition (77–79). Our data provide a rationale for therapeutic blockade of IRs to maintain an effective antileukemic immune milieu in CR patients and for overcoming the immunologic barriers to restoration of normal hematopoiesis in NR patients. Moreover, IR blockade together with activation of costimulatory pathways or pharmacological interventions such as inhibition of p38 mitogen–activated protein kinase, aimed at reactivating senescent T cells, may unleash superior antileukemia immunity (30, 36, 37, 80).

Methods

Human subjects and specimens. PB mononuclear cells (PBMCs) and/or BM mononuclear cells (BMMCs) were prospectively collected from AML patients (Supplemental Tables 7 and 8) and healthy volunteers (PB, $n = 56$; BM, $n = 24$; median age 40, range 19–69), and cryopreserved. Treatment response was assessed using standard criteria (80). CR was defined as <5% blasts in BM with neutrophil and platelet counts ≥1,000/μl and ≥100,000/μl, respectively. The sample size was based on the number of available paired specimens from the same patients before and after induction chemotherapy. All samples were flow cytometrically analyzed and gated in a blinded fashion. All data, including outliers, were included in analyses.

Flow cytometry. Flow cytometry was performed on a BD-LSRII (Becton Dickinson) and data were analyzed with FACSDiva V8.0.1 (BD) or FlowJo V10 (Tree Star). The LIVE/DEAD Fixable Aqua Dead Cell Stain Kit (Life Technologies) was used for all studies. Samples were preincubated with Human Trustain FC-Receptor Block (BioLegend) to prevent nonspecific antibody binding prior to staining for flow cytometric analysis. Antibodies and manufacturers are listed in Supplemental Table 10. The intracellular staining for GZMB, Ki67, T-bet, Eomes and cleaved caspase-3 was performed after cell permeabilization using the Intracellular Fixation & Permeabilization Buffer Set (eBioscience) as per manufacturer's instructions. High-dimensional single-cell analysis was performed using the viSNE bioinformatic tool (42) on the Matlab platform (MathWorks), and the CITRUS tool (82) on the R platform (supplemental methods).

In vitro experiments. PBMCs were thawed and divided into 2 aliquots, one used for flow cytometry and the other for FACS isolation or cytokine expression analysis. A DakoCytomation MoFlo (E1303A) (Beckman Coulter) was used to sort CD3+ T cells and leukemia blasts (CD45dim, SSClo). T cells were cultured alone, or in a 1:10 T cell/blast ratio (50,000 T cells/500,000 blasts per well), in a complete medium (RPMI 1640, 10% FCS, L-glutamine, and antibiotics) with or without IL-2 at 50 U/ml (Aldesleukin), and stimulated with Dynabeads Human T-activator CD3/CD28 (Life Technologies) as per manufacturer's instructions for 3 to 6 days before flow cytometric analysis. In designated experiments, the cells were also incubated for 6 days with anti–PD-1 mAb (10 μg/ml, Bristol-Myers Squibb, clinical grade, gift of C. Drake, Johns Hopkins University) or human recombinant OX40 ligand (1 μg/ml, BioLegend), counted, and analyzed by flow cytometry. For the cytokine expression assay, PBMCs were stimulated for 4 hours with 50 μg/ml PMA, 10 μg/ml brefeldin A, and 1 μM ionomycin (all from Sigma-Aldrich) prior to flow cytometry.

The cytotoxic effect of CD8+ T cells against primary AML cells was tested in vitro using anti–CD33/CD3 and control BiTE (cBiTE) antibody constructs (both provided by Amgen), as previously described (28, 29). Briefly, primary AML samples were sorted into CD8+CD57+ and CD8+CD57– T cells and AML blasts. T cells were then labeled with 2 μM CellVue Burgundy dye (eBioscience) and cultured with primary AML blasts (effector/target [E/T] ratio 1:1) in Iscoves' Modified Dulbecco's medium (Life Technologies) supplemented with 15% FBS, and 10 ng/ml each of IL-3, SCF, G-CSF, and GM-CSF (all Life Technologies),

for 48 hours. Cells were cultured with the addition of either BiTE (10 ng/ml) or cBiTE (10 μg/ml). After 48 hours, cell-specific cytotoxicity was determined using 4′,6-diamidino-2-phenylindole (DAPI) staining (CellVue Burgundy⁻ DAPI⁺) by flow cytometry.

Gene expression microarray experiments. PBMCs from 9 patients were used for microarray studies; 6 patients had paired pre- and postinduction samples analyzed (3 CR and 3 NR). As controls, we used PBMCs from 4 HCs matched for age, sex, and CMV status. PBMCs were first separated by T cell negative selection with a custom-made kit (Stem Cell Technologies) containing Abs against CD33, CD34, CD123, CD11c, and CD36. CD3⁺CD8⁺ T cells were sorted on a FACSAria II (BSL-2) (BD) to high purity (>98%; Supplemental Figure 7), and their RNA was isolated using TRIzol (Life Technologies) and purified using the RNA Clean & Concentrator Kit (Zymo Research). Sample quality was checked using the Agilent Bioanalyzer Nano kit, and concentrations were verified using the Nanodrop spectrophotometer (Thermo Fisher Scientific). Only specimens with a high RNA integrity number (RIN > 9) were used for analyses. Total RNA was amplified with the NuGEN Ovation Pico WTA system, followed by hybridization with Human PrimeView expression arrays (Affymetrix) as per manufacturer's instructions. Scanning was performed with an M10 scanner using AGCC ScanCom software. Microarray experiments were compliant with MIAME (Minimum Information About a Microarray Experiment), and raw and processed data were deposited in the NCBI's Gene expression Omnibus database (GEO GSE109179). Details on analyses are provided in the supplemental methods.

Statistics. For the initial cohort, untransformed T cell values were summarized using descriptive statistics and data presented on the raw scale. For the expanded AML and HC cohorts, a natural logarithmic transformation was applied to the T cell flow cytometry measurements, and comparisons between HCs and AML patients at diagnosis were modeled using standard linear regression models adjusted for age. Differences in log-transformed T cell subsets measurements from pretreatment to posttreatment between responders and NRs were estimated using a generalized, multivariable linear mixed-effects modeling framework (MLME). Specifically, log-scale T cell subset measurements were included as dependent terms in linear regression models with fixed effects for the time-point and response status, and random intercepts for each patient to account for within-patient clustering. Differential changes from pre- to posttreatment measurements between responders and NRs were assessed with an interaction term included in the model. The effect of the pretreatment patient and AML characteristics as well as effect of age (separately for HC and AML) on the CD8⁺ T cell composition (subsets) were examined using univariate linear regression models. Specifically, we estimated the proportion of variance explained by the characteristics using the R^2 statistic and associated P values from the linear regression model. The P values for each T cell subset were summarized and compared to a Bonferroni-adjusted significance threshold of $P < 0.05/30 = 0.00167$. See supplemental methods for additional statistical analyses.

Study approval. This study is complaint with Declaration of Helsinki principles and was conducted with prior approval of The Johns Hopkins Institutional Review Board (NA_00077575). All patients provided informed consent prior to inclusion in the study.

Address correspondence to: Leo Luznik, 1650 Orleans Street, CRB-1, Room 2M88, Baltimore, Maryland 21287, USA. Phone: 410.502.7732; Email: luznile@jhmi.edu. Or to: Ivana Gojo, 1650 Orleans Street, CRB-1, Room 346, Baltimore, Maryland 21287, USA. Phone: 410.502.8775; Email: igojo1@jhmi.edu.

1. Döhner H, et al. Diagnosis and management of AML in adults: 2017 ELN recommendations from an international expert panel. *Blood*. 2017;129(4):424–447.
2. Estey E. Acute myeloid leukemia: 2016 Update on risk-stratification and management. *Am J Hematol*. 2016;91(8):824–846.
3. Galluzzi L, Buqué A, Kepp O, Zitvogel L, Kroemer G. Immunological effects of conventional chemotherapy and targeted anticancer agents. *Cancer Cell*. 2015;28(6):690–714.
4. Zitvogel L, Galluzzi L, Smyth MJ, Kroemer G. Mechanism of action of conventional and targeted anticancer therapies: reinstating immunosurveillance. *Immunity*. 2013;39(1):74–88.
5. Knaus HA, et al. Immunomodulatory Drugs: Immune Checkpoint Agents in Acute Leukemia. *Curr Drug Targets*. 2017;18(3):315–331.
6. Alexandrov LB, et al. Signatures of mutational processes in human cancer. *Nature*. 2013;500(7463):415–421.
7. Austin R, Smyth MJ, Lane SW. Harnessing the immune system in acute myeloid leukaemia. *Crit Rev Oncol Hematol*. 2016;103:62–77.
8. Greiner J, et al. Mutated regions of nucleophosmin 1 elicit both CD4(+) and CD8(+) T-cell responses in patients with acute myeloid leukemia. *Blood*. 2012;120(6):1282–1289.
9. Chamuleau ME, et al. High INDO (indoleamine 2,3-dioxygenase) mRNA level in blasts of acute myeloid leukemic patients predicts poor clinical outcome. *Haematologica*. 2008;93(12):1894–1898.
10. Mussai F, et al. Acute myeloid leukemia creates an arginase-dependent immunosuppressive microenvironment. *Blood*. 2013;122(5):749–758.
11. Zhang L, et al. CD40 ligation reverses T cell tolerance in acute myeloid leukemia. *J Clin Invest*. 2013;123(5):1999–2010.
12. Buggins AG, et al. Microenvironment produced by acute myeloid leukemia cells prevents T cell activation and proliferation by inhibition of NF-κB, c-Myc, and pRb pathways. *J Immunol*. 2001;167(10):6021–6030.
13. Isidori A, et al. The role of the immunosuppressive microenvironment in acute myeloid leukemia development and treatment. *Expert Rev Hematol*. 2014;7(6):807–818.
14. Rezvani K, et al. T-cell responses directed against multiple HLA-A*0201-restricted epitopes derived from Wilms' tumor 1 protein in patients with leukemia and healthy donors: identification, quantification, and characterization. *Clin Cancer Res*. 2005;11(24 pt 1):8799–8807.
15. Greiner J, et al. Immune responses against the mutated region of cytoplasmatic NPM1 might contribute to the favorable clinical outcome of AML patients with NPM1 mutations (NPM1mut). *Blood*. 2013;122(6):1087–1088.
16. Horowitz MM, et al. Graft-versus-leukemia reactions after bone marrow transplantation. *Blood*. 1990;75(3):555–562.
17. Kolb HJ, et al. Graft-versus-leukemia effect of donor lymphocyte transfusions in marrow grafted patients. *Blood*. 1995;86(5):2041–2050.
18. Ersvaer E, et al. T cells remaining after intensive chemotherapy for acute myelogenous leukemia show a broad cytokine release profile including high levels of interferon-gamma that can be further increased by a novel protein kinase C agonist PEP005. *Cancer Immunol Immunother*. 2007;56(6):913–925.
19. Wendelbo Ø, Nesthus I, Sjo M, Paulsen K, Ernst P, Bruserud Ø. Functional characterization of T lymphocytes derived from patients with acute myelogenous leukemia and chemotherapy-induced leukopenia. *Cancer Immunol Immunother*. 2004;53(8):740–747.
20. Behl D, et al. Absolute lymphocyte count recovery after induction chemotherapy predicts superior survival in acute myelogenous leukemia. *Leukemia*. 2006;20(1):29–34.
21. Le Dieu R, et al. Peripheral blood T cells in acute myeloid leukemia (AML) patients at diagnosis have abnormal phenotype and genotype and form defective immune synapses with AML blasts. *Blood*. 2009;114(18):3909–3916.
22. Zhou Q, et al. Coexpression of Tim-3 and PD-1 identifies a CD8+ T-cell exhaustion phenotype in mice with disseminated acute myelogenous leukemia. *Blood*. 2011;117(17):4501–4510.
23. Zhang L, Gajewski TF, Kline J. PD-1/PD-L1 interactions inhibit antitumor immune responses in a murine acute myeloid leukemia model. *Blood*. 2009;114(8):1545–1552.
24. Kong Y, et al. PD-1(hi)TIM-3(+) T cells associate with and predict leukemia relapse in AML patients post allogeneic stem cell transplantation. *Blood Cancer J*. 2015;5:e330.
25. Kong Y, et al. T-Cell Immunoglobulin and ITIM domain (TIGIT) associates with CD8+ T-cell exhaustion and poor clinical outcome in AML patients. *Clin Cancer Res*. 2016;22(12):3057–3066.
26. Norde WJ, et al. PD-1/PD-L1 interactions contribute to functional T-cell impairment in patients who relapse with cancer after allogeneic stem cell transplantation. *Cancer Res*. 2011;71(15):5111–5122.
27. Schnorfeil FM, et al. T cells are functionally not impaired in AML: increased PD-1 expression is only seen at time of relapse and correlates with a shift towards the memory T cell compartment. *J Hematol Oncol*. 2015;8:93.
28. Krupka C, et al. Blockade of the PD-1/PD-L1 axis augments lysis of AML cells by the CD33/CD3 BiTE antibody construct AMG 330: reversing a T-cell-induced immune escape mechanism. *Leukemia*. 2016;30(2):484–491.
29. Laszlo GS, Gudgeon CJ, Harrington KH, Walter RB. T-cell ligands modulate the cytolytic activity of the CD33/CD3 BiTE antibody construct, AMG 330. *Blood Cancer J*. 2015;5:e340.
30. Akbar AN, Henson SM. Are senescence and exhaustion intertwined or unrelated processes that compromise immunity? *Nat Rev Immunol*. 2011;11(4):289–295.
31. Crespo J, Sun H, Welling TH, Tian Z, Zou W. T cell anergy, exhaustion, senescence, and stemness in the tumor microenvironment. *Curr Opin Immunol*. 2013;25(2):214–221.
32. Schietinger A, Greenberg PD. Tolerance and exhaustion: defining mechanisms of T cell dysfunction. *Trends Immunol*. 2014;35(2):51–60.

33. Zarour HM. Reversing T-cell dysfunction and exhaustion in cancer. *Clin Cancer Res*. 2016;22(8):1856–1864.

34. Legat A, Speiser DE, Pircher H, Zehn D, Fuertes Marraco SA. Inhibitory receptor expression depends more dominantly on differentiation and activation than "exhaustion" of human CD8 T cells. *Front Immunol*. 2013;4:455.

35. Maecker HT, McCoy JP, Nussenblatt R. Standardizing immunophenotyping for the Human Immunology Project. *Nat Rev Immunol*. 2012;12(3):191–200.

36. Henson SM, et al. p38 signaling inhibits mTORC1-independent autophagy in senescent human CD8+ T cells. *J Clin Invest*. 2014;124(9):4004–4016.

37. Akbar AN, Henson SM, Lanna A. Senescence of T lymphocytes: implications for enhancing human immunity. *Trends Immunol*. 2016;37(12):866–876.

38. Apetoh L, et al. Consensus nomenclature for CD8+ T cell phenotypes in cancer. *Oncoimmunology*. 2015;4(4):e998538.

39. Kared H, Martelli S, Ng TP, Pender SL, Larbi A. CD57 in human natural killer cells and T-lymphocytes. *Cancer Immunol Immunother*. 2016;65(4):441–452.

40. Wherry EJ. T cell exhaustion. *Nat Immunol*. 2011;12(6):492–499.

41. Chauvin JM, et al. TIGIT and PD-1 impair tumor antigen-specific CD8+ T cells in melanoma patients. *J Clin Invest*. 2015;125(5):2046–2058.

42. Amir el-AD, et al. viSNE enables visualization of high dimensional single-cell data and reveals phenotypic heterogeneity of leukemia. *Nat Biotechnol*. 2013;31(6):545–552.

43. Henson SM, Macaulay R, Riddell NE, Nunn CJ, Akbar AN. Blockade of PD-1 or p38 MAP kinase signaling enhances senescent human CD8(+) T-cell proliferation by distinct pathways. *Eur J Immunol*. 2015;45(5):1441–1451.

44. Nunes C, Wong R, Mason M, Fegan C, Man S, Pepper C. Expansion of a CD8(+)PD-1(+) replicative senescence phenotype in early stage CLL patients is associated with inverted CD4:CD8 ratios and disease progression. *Clin Cancer Res*. 2012;18(3):678–687.

45. Zelle-Rieser C, et al. T cells in multiple myeloma display features of exhaustion and senescence at the tumor site. *J Hematol Oncol*. 2016;9(1):116.

46. Brenchley JM, et al. Expression of CD57 defines replicative senescence and antigen-induced apoptotic death of CD8+ T cells. *Blood*. 2003;101(7):2711–2720.

47. Verma K, et al. Human CD8+ CD57− TEMRA cells: Too young to be called "old". *PLoS One*. 2017;12(5):e0177405.

48. Blackburn SD, et al. Coregulation of CD8+ T cell exhaustion by multiple inhibitory receptors during chronic viral infection. *Nat Immunol*. 2009;10(1):29–37.

49. Huang AC, et al. T-cell invigoration to tumour burden ratio associated with anti-PD-1 response. *Nature*. 2017;545(7652):60–65.

50. Saverino D, et al. The CD85/LIR-1/ILT2 inhibitory receptor is expressed by all human T lymphocytes and down-regulates their functions. *J Immunol*. 2000;165(7):3742–3755.

51. Borrego F. The CD300 molecules: an emerging family of regulators of the immune system. *Blood*. 2013;121(11):1951–1960.

52. Quigley M, et al. Transcriptional analysis of HIV-specific CD8+ T cells shows that PD-1 inhibits T cell function by upregulating BATF. *Nat Med*. 2010;16(10):1147–1151.

53. Björkström NK, et al. CD8 T cells express randomly selected KIRs with distinct specificities compared with NK cells. *Blood*. 2012;120(17):3455–3465.

54. Strauss-Albee DM, Horowitz A, Parham P, Blish CA. Coordinated regulation of NK receptor expression in the maturing human immune system. *J Immunol*. 2014;193(10):4871–4879.

55. Wherry EJ, Kurachi M. Molecular and cellular insights into T cell exhaustion. *Nat Rev Immunol*. 2015;15(8):486–499.

56. Henson SM, Akbar AN. KLRG1 — more than a marker for T cell senescence. *Age (Dordr)*. 2009;31(4):285–291.

57. Wood WA, et al. Chemotherapy and stem cell transplantation increase p16INK4a expression, a biomarker of T-cell aging. *EBioMedicine*. 2016;11:227–238.

58. Doering TA, Crawford A, Angelosanto JM, Paley MA, Ziegler CG, Wherry EJ. Network analysis reveals centrally connected genes and pathways involved in CD8+ T cell exhaustion versus memory. *Immunity*. 2012;37(6):1130–1144.

59. Bindea G, et al. ClueGO: a Cytoscape plug-in to decipher functionally grouped gene ontology and pathway annotation networks. *Bioinformatics*. 2009;25(8):1091–1093.

60. Chen L, Flies DB. Molecular mechanisms of T cell co-stimulation and co-inhibition. *Nat Rev Immunol*. 2013;13(4):227–242.

61. Xing S, et al. Tcf1 and Lef1 transcription factors establish CD8(+) T cell identity through intrinsic HDAC activity. *Nat Immunol*. 2016;17(6):695–703.

62. Castro MA, et al. Extracellular isoforms of CD6 generated by alternative splicing regulate targeting of CD6 to the immunological synapse. *J Immunol*. 2007;178(7):4351–4361.

63. Willinger T, Freeman T, Hasegawa H, McMichael AJ, Callan MF. Molecular signatures distinguish human central memory from effector memory CD8 T cell subsets. *J Immunol*. 2005;175(9):5895–5903.

64. Duraiswamy J, et al. Phenotype, function, and gene expression profiles of programmed death-1(hi) CD8 T cells in healthy human adults. *J Immunol*. 2011;186(7):4200–4212.

65. Baitsch L, et al. Exhaustion of tumor-specific CD8+ T cells in metastases from melanoma patients. *J Clin Invest*. 2011;121(6):2350–2360.

66. Parish IA, et al. The molecular signature of CD8+ T cells undergoing deletional tolerance. *Blood*. 2009;113(19):4575–4585.

67. Gros A, et al. PD-1 identifies the patient-specific CD8+ tumor-reactive repertoire infiltrating human tumors. *J Clin Invest*. 2014;124(5):2246–2259.

68. Fourcade J, et al. CD8(+) T cells specific for tumor antigens can be rendered dysfunctional by the tumor microenvironment through upregulation of the inhibitory receptors BTLA and PD-1. *Cancer Res*. 2012;72(4):887–896.

69. Horton BL, Gajewski TF. Back from the dead: TIL apoptosis in cancer immune evasion. *Br J Cancer*. 2018;118(3):309–311.

70. Bachireddy P, et al. Reversal of in situ T-cell exhaustion during effective human antileukemia responses to donor lymphocyte infusion. *Blood*. 2014;123(9):1412–1421.

71. Riches JC, et al. T cells from CLL patients exhibit features of T-cell exhaustion but retain capacity for cytokine production. *Blood*. 2013;121(9):1612–1621.

72. Fucikova J, et al. Calreticulin exposure by malignant blasts correlates with robust anticancer immunity and improved clinical outcome in AML patients. *Blood*. 2016;128(26):3113–3124.

73. Greiner J, et al. Acute myeloid leukemia with mutated nucleophosmin 1 — an immunogenic AML subtype and potential candidate for immune checkpoint inhibition [published online ahead of print September 2017]. *Haematologica*. doi: 10.3324/haematol.2017.176461.

74. Brodin P, Davis MM. Human immune system variation. *Nat Rev Immunol*. 2017;17(1):21–29.

75. Brodin P, et al. Variation in the human immune system is largely driven by non-heritable influences. *Cell*. 2015;160(1–2):37–47.

76. Topalian SL, Taube JM, Anders RA, Pardoll DM. Mechanism-driven biomarkers to guide immune checkpoint blockade in cancer therapy. *Nat Rev Cancer*. 2016;16(5):275–287.

77. Williams P, et al. Checkpoint expression by acute myeloid leukemia (AML) and the immune microenvironment suppresses adaptive immunity. *Blood*. 2017;130(suppl 1):185.

78. Zeidan AM, et al. A multi-center phase I trial of ipilimumab in patients with myelodysplastic syndromes following hypomethylating agent failure. *Clin Cancer Res*. 2018;24(15):3519–3527.

79. Zeidner JF, et al. Phase II study of high dose cytarabine followed by pembrolizumab in relapsed/refractory acute myeloid leukemia (AML). Blood. 2017;130(suppl 1):1349.

80. Lanna A, Henson SM, Escors D, Akbar AN. The kinase p38 activated by the metabolic regulator AMPK and scaffold TAB1 drives the senescence of human T cells. *Nat Immunol*. 2014;15(10):965–972.

81. Cheson BD, et al. Revised recommendations of the International Working Group for Diagnosis, Standardization of Response Criteria, Treatment Outcomes, and Reporting Standards for Therapeutic Trials in Acute Myeloid Leukemia. *J Clin Oncol*. 2003;21(24):4642–4649.

82. Bruggner RV, Bodenmiller B, Dill DL, Tibshirani RJ, Nolan GP. Automated identification of stratifying signatures in cellular subpopulations. *Proc Natl Acad Sci U S A*. 2014;111(26):E2770–E2777.